Classifying minimally-disabled multiple sclerosis patients from resting-state functional connectivity☆

Jonas Richiardi[a,b,*], Markus Gschwind[a,d], Samanta Simioni[e], Jean-Marie Annoni[a,d], Beatrice Greco[c], Patric Hagmann[e,f], Myriam Schluep[e], Patrik Vuilleumier[a,d], Dimitri Van De Ville[a,b]

[a] *University of Geneva, Switzerland*
[b] *École Polytechnique Fédérale de Lausanne (EPFL), Switzerland*
[c] *Merck-Serono, Geneva, Switzerland*
[d] *Geneva University Hospital (HUG), Switzerland*
[e] *Lausanne University Hospital (CHUV), Switzerland*
[f] *University of Lausanne, Switzerland*

Keywords: brain decoding, brain networks, classification, functional magnetic resonance imaging, imaging marker

*Corresponding author. Address: EPFL / IBI-STI / GRVDV, Station 17, 1015 Lausanne, Switzerland. Phone: +41-21-6939610. Email jonas.richiardi@epfl.ch

Multiple sclerosis (MS) is a common neurological disease, especially among the young in northern countries and is characterized by recurrent or progressive inflammatory events that lead to spatially disseminated demyelination of the central nervous system, followed by subsequent axonal loss (Compston and Coles, 2008). Early treatment is important to avoid permanent damage and might slow or delay progression (Jacobs et al., 2000; Kappos et al., 2007). However, due to the variety of clinical presentations and its large differential diagnosis, early identification of the disease is especially problematic (Rolak and Fleming, 2007; Swanton et al., 2007). In its most common relapsing-remitting form (RRMS), patients present attacks alternating with episodes of clinical improvements, following an unpredictable rhythm (Noseworthy et al., 2000). Current diagnostic workup is based on clinical examination together with structural magnetic resonance imaging (MRI) of brain and spine as well as cerebrospinal fluid analysis, seeking for evidence of both *dissemination in time* and *dissemination in space* of the inflammatory lesions (Compston and Coles, 2008). The role of MRI, most often relying on T2-weighted and Gadolinium-enhanced images to establish the diagnosis, is of growing importance to establish the diagnosis and follow disease progression or remission (Polman et al., 2005; Barkhof et al., 2009; Polman et al., 2011). However, conventional MRI has several recognised limitations; the "hidden" damage known to occur in the normal appearing brain tissue (NABT) (Fu et al., 1998) is not captured; structural lesions are not always specific to MS (Barkhof and Filippi, 2009); T2 hyperintensities are histologically unspecified since inflammation and demyelination as well as axonal damage and gliosis have similar signal characteristics (Ratchford and Calabresi, 2008); and the correlation of lesion load and clinically significant impairment is poor (Barkhof, 2002; Filippi and Agosta, 2010). Therefore, current radiological signs obtained from structural MRI may not reflect the actual disease state.

In this context, interest is growing for alternative MRI modalities, that may provide complementary information, with the aim of finding additional imaging markers for MS (Filippi and Agosta, 2010). One such modality is diffusion MRI: there is evidence that axial diffusion is relatively specific to axonal degeneration (Song et al., 2003), while increased radial diffusion is mainly driven by demyelination (Budde et al., 2009; Zhu et al., 1999). The use of advanced tractography methods suggests that a connectional framework may lead to improved sensitivity and specificity to the disease and its related clinical impairment (Ciccarelli et al., 2005; Lin et al., 2005; Dineen et al., 2009).

Another technique that also builds on the connectional framework and has potential sensitivity to detect "invisible" lesions is functional MRI (fMRI). Based on the blood oxygen level dependent (BOLD) signal, this technique gives an indirect measure of aggregate neuronal excitation-inhibition in grey matter microcircuits (Logothetis, 2008). MS lesions can alter neuronal networks in several ways. Several fMRI studies have highlighted brain circuit plasticity and its potentially adaptive role in recovery or compensation in response to brain lesions (Reddy et al., 2000b), for motor (e.g. finger tapping) (Lee et al., 2000; Reddy et al., 2000a; Morgen et al., 2004) as well as cognitive tasks (e.g. working memory and attention tasks) (Mainero et al., 2004; Morgen et al., 2007). While permanent axonal changes already accompany even early acute inflammatory responses (Trapp et al., 1998), fMRI studies indicate that adaptive plasticity might limit the initial clinical expression of the disease (Cifelli and Matthews, 2002; Rocca and Filippi, 2007) and that patients can show complete clinical

recoveries after relapses, explaining the missing link between clinical and radiological presentation. Pathological functional effects have been shown, as for example the loss of interhemispheric inhibition, related to corpus callosum atrophy (Manson et al., 2006, 2008). A negative effect of disease progression on plasticity has also become clear, limiting the potential for adaptive capacity and leading to globally reduced brain connectivity and dysfunction (Morgen et al., 2004; Cader et al., 2006).

Furthermore, beyond local changes in activity, fMRI can provide information on the architecture and interconnectivity of more distributed brain networks, notably by measuring patterns of spontaneous fluctuations during resting state (Biswal et al., 1995; Greicius et al., 2003). Resting-state connectivity analysis has benefitted from recent advances in fMRI methodology allowing to investigate intrinsic (i.e. not task related) brain activity across the whole brain and to identify the degree of functional correlation between distant areas (Greicius et al., 2009). Many publications have focused on analysing the default-mode network (DMN) (Buckner et al., 2008), a set of regions highly synchronised during rest. This methodology has been used in several diseases characterised by diffuse lesions (Fox and Greicius, 2010) such as schizophrenia (Jafri et al., 2008), Alzheimer's disease (Li et al., 2002; Greicius et al., 2004) or depression (Greicius et al., 2007), but investigations in MS are limited to relatively fewer publications. For example, Cover et al. (2006) found decreased inter-hemispheric connectivity in MS patients at rest, using a coherence measure based on magneto-encephalography (MEG). Rocca et al. (2010) found reduction of activity in the anterior cingulate cortex (ACC) at rest in MS patients relative to controls, and in cognitively impaired MS patients related to cognitively intact MS patients. Weaker DMN connectivity in the ACC of MS patients was also reported by Bonavita et al. (2011) using independent component analysis of fMRI resting-state data. Roosendaal et al. (2010) investigated fMRI resting-state networks in patients with clinically isolated syndrome (CIS) and patients with RRMS and observed an increased synchronisation of some resting-state networks in CIS patients which disappeared in those with RRMS, suggesting initial functional compensation that is lost with disease progression. Using ICA and seed correlation, Jones et al. (2011) showed significant differences in connectivity at rest between a single MS patient with an important thalamic lesion and a group of controls, in particular in the default mode network.

Based on these studies, resting-state fMRI offers a promising avenue to further investigate the functional impact of pathology, including at early stages of MS where long-range connectivity can be altered by both inflammatory processes and mild axonal damage. However, a comprehensive assessment of altered brain connectivity would need to detect subtle and distributed patterns throughout the brain, in a data-driven and objective manner despite the highly variable location of lesions in MS. Moreover, for both task-based activity and resting-state connectivity analyses, functional changes and compensatory mechanisms can appear either as increases or decreases, depending on the task, individual patient, and/or disease state. Given the high number of possible connections to test, mass-univariate or summary statistics have difficulties to find significant differences; e.g., mean connectivity between specific regions of interest may show no consistent differences between MS and controls (Lowe et al., 2008). Instead, here we propose the use of *predictive* multivariate models that can generalise to unseen subjects (those not used to learn the parameters of a model) and

thus potentially lead to a new imaging-based marker for MS. Recent work has highlighted the feasibility of using single structural scans for reliable MS diagnosis (Rovira et al., 2009), the ability of local multivariate predictive methods to discriminate between MS patients and controls with high accuracy, even when using NABT structural data (Weygandt et al., 2011), and the possibility of using global multivariate methods with structural data to distinguish various aspects of MS severity (Bendfeldt et al., 2012). Accordingly, given the increased use and development of predictive modelling techniques in fMRI research, originally derived from machine learning or pattern recognition (Kamitani and Tong, 2005; Mourao-Miranda et al., 2005; Ethofer et al., 2009; Weil and Rees, 2010; Shirer et al., 2011), it would appear highly suitable and advantageous to apply similar techniques to characterise high-dimensional fMRI data obtained during resting-state (Richiardi et al., 2010, 2011). There has also been a slow concurrent increase in the use of multivariate predictive modelling techniques applied to functional connectivity data of pathological subjects. For example, Craddock et al. (2009) have proposed using the temporal pairwise correlations between 15 expertly selected regions of interest as features for a support vector machine classifier applied to depressive patients. More recently, Chen et al. (2011) have used a low-dimensional representation of connectivity differences obtained from non-parametric hypothesis testing and linear discriminant analysis to classify Alzheimer's disease patients, MCI patients, and normal subjects. To our knowledge, however, no multivariate predictive modelling approach based on functional connectivity has been reported in MS.

Here, we describe a functional connectivity analysis of resting-state data adapted from our recently developed multivariate connectivity decoding technique (Richiardi et al., 2011), which we use to discriminate between minimally-disabled MS patients (median EDSS 2.0) and healthy controls, a first step towards the development of predictive prognosis models. Our approach exploits whole-brain data rather than restricting the study to a few regions of interest such as motor cortices or the DMN. By doing so, we aim at exploring global connectivity changes in MS and defining which functional connections are particularly affected by the disease. Beyond the data-driven exploration of the functional impact of distributed connectivity damage associated with MS, our method provides a classifier model that gives predictive information on individual status (as opposed to whole-group analysis based on a priori classification). The ability to classify patients based on fMRI connectivity patterns is a first step towards developing useful tools for improving the diagnostic workup and the monitoring and prognosis of MS patients, even in the absence of overt clinical signs or visible structural lesions.

1. Materials and Methods

1.1. Subjects and task

Twenty-two relapsing-remitting (RR) MS patients according to McDonald's diagnostic criteria (Polman et al., 2005) were selected from our outpatient clinic database. The selection criteria were: (1) mild to moderate neurological disability but unimpaired ambulation (Expanded Disability Status Scale (EDSS) ≤ 2.5 in all cases (Kurtzke, 1983)); (2) no clinical relapse and no corticosteroid therapy for at least 6 weeks before inclusion in the study; and (3) no other

neurological diagnosis, major depression, or psychiatric illness according to the DSM-IV criteria. All underwent a similar MRI protocol during their follow-up, with all parameters of the imaging sequence equal and with the same MRI scanner in all subjects, in order to prevent confounding factors in the analysis. All patients were only minimally disabled (median EDSS 2, range 1.5 to 2.5), with five subjects having had a single attack at the time of imaging. At the time of scanning, 11 out of 22 patients were receiving disease-modifying therapies (interferon β-1a or 1b in 9 cases, glatiramer acetate in 2 cases) for a mean duration of 38.8 $\pm$ 37.1 months).

The control group consisted of 14 healthy subjects with no history of alcohol or drug abuse, major psychiatric disorder (major depression, psychosis, untreated bipolar disorders), head trauma, other neurological disorder, or systemic illness.

The characteristics of the study population are summarised in Table 1, and full details are provided in Supplementary Table 1.

	patients (N=22)	controls (N=14)
gender (M/F)	8/14	5/9
mean age at inclusion (SD)	36.8 (7.9)	38.4 (6)
median EDSS (range)	2.0 (1.5-2.5)	-
mean years of disease duration (SD)	4.7 (3.5)	-

Table 1: Demographic information of the study population

The study was approved by the local university Ethics Committee, and all subjects gave informed consent for their participation in accordance with the Declaration of Helsinki.

1.2. Data acquisition

Data was acquired on a Siemens 3T TrioTIM (VB15) platform, using a 32-channel head coil. Functional imaging data were acquired in one session using gradient-echo echo-planar imaging (TR/TE/FA = 1.1s/27ms/90°, matrix = 64×64, voxel size = 3.75×3.75×5.63mm^3, 21 contiguous transverse slices, 450 volumes). Longitudinal magnetisation was assumed to reach steady-state after approximately 10-11 seconds, and the first 10 scans of each acquisition were discarded. In total, $T = 440$ volumes were kept for analysis. The resting state scanning took 8 minutes. Participants were instructed to lie still with their eyes closed, to relax and let their mind wander without doing anything in particular (as is standard practice in resting-state fMRI studies (Fox and Raichle, 2007; Mantini et al., 2007; Helekar et al., 2010)).

A structural image was also acquired using a high resolution three-dimensional T1-weighted MPRAGE sequence (160 slices, TR/TE/FA = 2.4 s/2.98 ms/9°, matrix = 256 × 240, voxel size = 1 × 1 × 1.2mm^3).

In addition, a turbo spin-echo proton density (PD) image (46 slices, TR/FA = 2640 ms/150°, matrix = 204 × 256, voxel size = 0.98 × 0.98 × 3mm^3) was acquired for lesion tracing.

1.3. Data processing and construction of the functional connectivity matrix

1.3.1. Lesion masks and lesion load computation

Lesions were traced manually on the PD image by 2 independent radiologists (Medical Image Analysis Center, University Hospital Basel, E.W. Radue). Le-

sion load was calculated by multiplying the total number of traced lesion voxels by the voxel volume.

1.3.2. Structural and Resting-state data

To extract the resting-state functional connectivity matrix, we follow the methodology described in previous work (Achard et al., 2006; Richiardi et al., 2011). Supplementary Section 1 provides an overview of the processing pipeline.

For each subject, the functional data is spatially realigned and motion-corrected to the mean image with SPM8 (least-square technique with rigid body and quadratic interpolation). Movement parameters are checked for excessive translation and rotation, and the volumes inspected visually for intensity spikes, which are due to the spin-history effect in case of large movement (Friston et al., 1996). One patient (not included in Table 1) was excluded due to excessive movement.

Each subject's structural image is normalised to MNI space and segmented using the SPM8 (`http://www.fil.ion.ucl.ac.uk/spm/`) *new segmentation* algorithm, an updated version of the unified segmentation algorithm (Ashburner and Friston, 2005). The structural image is co-registered to the mean image of the functional data. An individual brain atlas containing 90 cortical and subcortical regions of interest (ROIs) is then computed with a modified version of the IBASPM toolbox (Alemán-Gómez et al., 2006) and the AAL atlas (Tzourio-Mazoyer et al., 2002). A full list of these regions is provided in Supplementary Table 2. This structural atlas is then mapped back onto the native resolution of the functional data, the time-series are linearly detrended, and region-averaged time series are obtained. These regional time-series are windsorised to the 95th percentile to increase robustness to outliers. At this stage, each subject's functional data is contained in a $90 \times T$ matrix (multivariate time series).

The regional time courses are then filtered into frequency subbands using a wavelet transform (cubic orthogonal B-spline wavelets). The subband of interest for this study contains frequencies in the 0.06–0.11 Hz range, to focus on resting-state activity (Richiardi et al., 2011). While the commonly used freeuency band is wider (Biswal et al., 1995; Lowe et al., 1998), the use of wavelet correlation (Achard et al., 2006) relies on a dyadic wavelet decomposition, where the influence of boundary conditions becomes more important as we move to coarser (lower frequency) subbands. Given the available acquisition time, the current subband is theoretically a good compromise between boundary condition artefacts (getting worse towards lower frequencies because there are fewer independent samples) and signal-to-noise ratio (getting worse towards higher frequencies because of the haemodynamic response acting as a low-pass filter). To further ensure that the time course noise (due to movement or scanning artefacts) does not add a confound and is equal between control and subject groups, the average standard deviation of the regional filtered time courses $\bar{\sigma}_R$ is computed for each subject, and a Kruskal-Wallis test is conducted on the hypothesis of no difference in median value of $\bar{\sigma}_R$ between groups.

After computing pairwise Pearson correlations between all ROIs in the atlas, a 90×90 correlation matrix is obtained for each subject. Note that for the whole procedure, the data of each subject is not influenced by the data of other subjects; e.g., no groupwise registration is used. This will ensure independence later on in the modelling stage, and allows a proper deployment of predictive approach.

1.4. Modelling and classification of connectivity matrices

The functional connectivity matrix can be considered as the *adjacency matrix* of an undirected, weighted, complete graph, by removing the diagonal elements. This defines the *connectivity graph*, where each atlas ROI corresponds to a vertex and the strength of functional connectivity between two ROIs is encoded in the edge weight (a correlation coefficient). To permit the use of machine learning algorithms, we use the direct graph embedding method (Richiardi et al., 2010), in which the upper-triangular part of the adjacency matrix is lexicographically organized in a vector representation. This provides a flexible approach enabling us to model the whole-brain graph, or to examine a specific hemisphere or lobe, or even to consider connections inside functionally-defined networks. These types of sub-graphs can be readily extracted from the full adjacency matrix, and represented as vectors. It is possible to train the classifier on the whole graph, and then to study the relative discriminative importance (weights, see below) of various subgraphs, or to directly train the classifier on subgraphs. In the remainder of this work we focus on the former method. Thus, at this stage, each subject's resting-state data is represented by a feature vector whose elements are pairwise regional correlation coefficients. We point out that the input features used in Craddock et al. (2009) are equivalent to our direct embedding approach, the difference being the addition of a Fisher R-to-Z transform step and the lower dimensionality of the feature space generated (15 regions lead to 105 edge weights in feature space).

For classification, we use an ensemble of functional trees (Richiardi et al., 2011), a variation on the random forest scheme occasionally used in neuroimaging (Langs et al., 2011). This classifier yields a *discriminative weight* w_i for each functional connection in our resting-state data. This value represents the relative ability of each connection to discriminate between controls and MS patients. Their interpretation is very close to that of regression coefficients, except that they only make sense as part of a multivariate pattern: connections with high discriminative weight are useful in predicting patient status (they are a good predictor), while connections with low discriminative weight carry little information. After permutation testing to remove connections with insignificant discriminative weights, the set of remaining connections yields what we call a *discriminative graph*. The discriminative weight of each connection can then be used to compute *regional discriminative weights* by summing the discriminative weights of all connections attached to a particular region. The regions and connections of the discriminative graph can be represented in MNI space. By visualising the connections and regions that are jointly most discriminative (those from which a prediction of the MS status of any new subject can be made), we can obtain a map of all connections driving the classification between patient and control groups. Supplementary Section 1 contains more details of about the computation of discriminative weights, including the permutation testing approach used for statistical control.

In order to evaluate the performance and generalisation ability of the classifier, we adopt a leave-one-subject-out cross-validation approach, whereby the dataset is split N times into a training set containing $N - 1$ subjects and a test set containing 1 subject. The training set is used for learning the classifier parameters, while the held-out testing set is used for prediction. We can then measure how well the classifier is performing by aggregating prediction results across the cross-validation folds.

We report the classification performance using the familiar measures *sensitivity* and *specificity*. Supplementary Section 7 contains more details about the computation of performance measures.

1.5. Summary indices of connectivity alterations

We can divide the set of connections C that provide discrimination between controls and MS patients into two distinct, non-overlapping parts: connections that are, on average, weaker in patients than in controls ($C\_$), and those that are stronger (C_+). Thus, we have $C = C\_ \cup C_+$, and $C\_ \cap C_+ = \varnothing$. Then, we can compute two summary measures per subject, which can serve for post-hoc comparison of the results between groups.

For each subject s, the *increased connectivity index* (ICI) is the sum of correlation values of the connections in C_+, denoted ρ_i^s, each multiplied by its normalised discriminative weight $\hat{w}_i = \frac{w_i}{||\mathbf{w}||_1}$. Thus, we have $ICI^s = \sum_{j \in C_+} \rho_j^s \hat{w}_j$. The *reduced connectivity index* (RCI) is computed in the same way, but from the set of connections that are weaker in patients, $C\_$; that is for each subject, $RCI^s = \sum_{j \in C\_} \rho_j^s \hat{w}_j$. These two different indices can be plotted jointly to provide a simple two-dimensional view of discriminative connectivity alterations in MS patients with respect to controls, e.g. subject 4 would be plotted in $\mathbb{R}^2$ as (RCI^4, ICI^4). Figure 1 of the results section provides an example.

Additionally, for statistical analysis we may want to remove the bias due to total edge strength of the connectivity graph (sum of edge weights $\sum_i \rho_i^s$), which can vary considerably between subjects, and we can compute the normalised RCI, respectively ICI, as $nRCI^s = \frac{1}{\sum_i \rho_i^s} RCI^s$. This reflects the discriminative importance and connection strength in the discriminative (sub)graph with respect to the total edge strength of the connectivity graph.

These indices are different from a simple averaging of correlation values, because only a discriminative subset of connections is used, and the sum is weighted by the discriminative importance of each connection. We should also point out that Chen et al. (2011) have previously defined a "decreased connectivity index" and an "increased connectivity index". While related to our ICI and RCI, these are different from our indices. They are computed from an "increased connection set" (respectively decreased) which is the set of connections whose z-scores, obtained from a Wilcoxon rank-sum test between groups, are the n most positive (respectively negative). Within the increased (respectively decreased) connection set, the correlation values are averaged, forming the indices. Furthermore, they are used as input features to an LDA classifier in that paper, as opposed to being a post-hoc summary measure of a high-dimensional discrimination function in our approach.

2. Results

2.1. Predictive modelling of whole-brain resting-state functional connectivity patterns has high sensitivity for MS

The pattern of correlation coefficients between all pairs of ROIs was calculated for each subject in the MS and control groups, and submitted to our multivariate decoding algorithm to determine the most consistent differences in the low-frequency functional connectivity in resting-state between the two groups.

After cross-validation, 18 out of 22 patients and 12 out of 14 controls were classified correctly. These results correspond to a sensitivity of 82% (above chance at $p < 0.005$, Wilson's method for the binomial distribution), and a specificity of 86% (above chance at $p < 0.01$). Importantly, these classification results are not driven by noise differences between patients and controls, as indicated by calculating the standard deviation of the regional filtered time-courses $\bar{\sigma}_R$ (p=0.24, Kruskal-Wallis test on the null hypothesis of no difference in median value of $\bar{\sigma}_R$ between groups).

When looking at the misclassified patients (details in Supplementary Table 1), it can be seen that two of them had only a single attack preceding their inclusion in our study, and a lesion load in the lowest quartile of our sample (0.39 and 0.51 cm^3). The two other misclassified patients had an EDSS score of 1.5, i.e. the lowest in our database. This suggests that a potential source of classification errors might concern the minimal disability caused by the disease, when lesion load still has little or no impact on global functional connectivity. Regarding patient treatment, it seems to have no effect on the performance of the classification algorithm, but the sample size is not sufficient to assert this with confidence.

Figure 1 shows the scatterplot of the increased and reduced connectivity indices (ICI and RCI) computed post-hoc on the whole-group (see method described in Section 1.5). This representation, where each index is based on a distinct sub-network of the discriminative graph, reveals good separation between the groups. This suggests that the discriminative graph can indeed successfully capture a predictive subset of connections, and that the discriminative weight is reliably estimated across different subjects. As shown in this figure, misclassified patients are generally in the region of the RCI/ICI graph corresponding to high connectivity for patients, both in the C_- and C_+ subnetworks. This entails these patients tend to exhibit stronger connectivity with respect to controls than the classifier expected from the training sample. Likewise, the misclassified controls tend to be those with the weakest connectivity in both the C_- and C_+ subnetworks.

Interestingly, there is a significant positive correlation between nRCI (see Section 1.5) and the lesion load computed in MNI space (robust correlation coefficient (Rousseeuw and Driessen (1998)) : 0.61; IRWLS robust linear regression: $p < 0.001$ to reject the null hypothesis of a zero slope coefficient). This suggests that, while total edge strength ($\sum_i \rho_i^s$, computed over the whole connectivity graph for each subject) might not be a good indicator of lesions (non-significant correlation between the vector whose elements are the total edge strengths from all patients and the vector whose elements are the corresponding lesion load values from all patients), the effect of white matter lesion can be observed within a small subgraph (part of the discriminative subgraph) learned on resting-state connectivity, linking known physiological effects of the disease with functional MRI connectivity measurements. Indeed, this finding may be taken as evidence that discriminative functional connectivity changes can at least partly be attributed to white matter lesions. Furthermore, although no causal mechanism is clear, this may indicate that connectivity strength of the C_- subgraph relative to the rest of the network is increased in these minimally disabled patients in an effort to compensate for increasing lesion load, while still being below the connectivity strength of controls.

Supplementary Table 4 contains the weight of all connections that make up

the two indices. For an anatomical representation of subgraphs corresponding to the ICI and RCI, see Figure 4 (section 2.2 below).

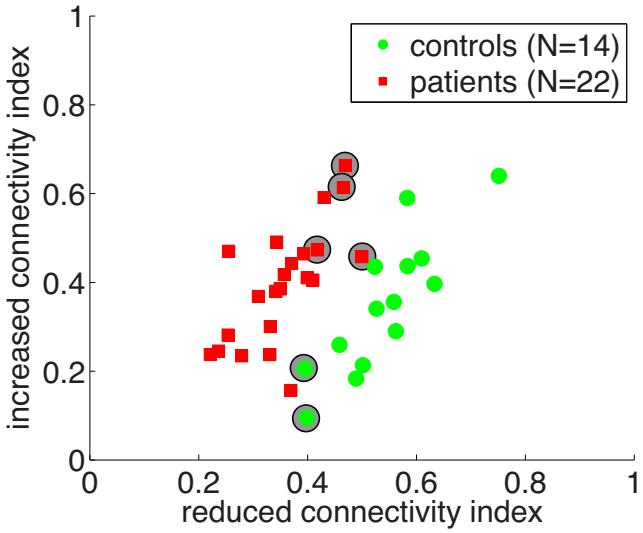

Figure 1: Scatterplot of reduced and increased connectivity indices for controls (green circles) and patients (red squares). This is a summary representation of the pattern of connectivity alterations that is predictive of MS in our sample, computed post-hoc on the whole dataset. Points corresponding to subjects misclassified by our decoding algorithm in the leave-one-out cross-validation procedure are circled in grey.

2.2. Connections distinguishing MS from controls at rest form a large-scale network with low edge density

To visualise the anatomical organisation of connectivity changes (see Section 1.4), we first extract the *discriminative graph* indicating which connections and regions are jointly most discriminative between controls and MS patients. In this sample we find 161 connections (out of 4005) that have significant discriminative weights ($p<0.05$, corrected for multiple comparisons by permutation testing), corresponding to an edge density (connectance) $\mathcal{D} = \frac{161}{4005} \approx 0.04$. Since $\mathcal{D} \ll 1$, we interpret the discriminative graph as having a low edge density. The connections with significant discriminative weights are shown in Figure 2. The size of the ROIs spheres and connection paths is proportional to the number of times a connection to or from a region is selected for classification during cross-validation, and how discriminative it is between the groups. Note that since the method is multivariate, these connections are not discriminative on their own, but rather, the joint set of connections is discriminative.

The overall pattern of changes reveals a network of functional connections mainly centred on subcortical and fronto-parieto-temporal regions, consistent with the typically widely distributed lesions in MS. However, different patterns can be seen in different parts of the brain. A notable feature is that occipital regions are not particularly important in the differentiation of MS from control brains, even though visual networks often constitute a distinctive component of resting state activity in normal conditions (Raichle et al., 2001; Salvador et al., 2005; Mantini et al., 2007). The frontal lobe contains relatively few

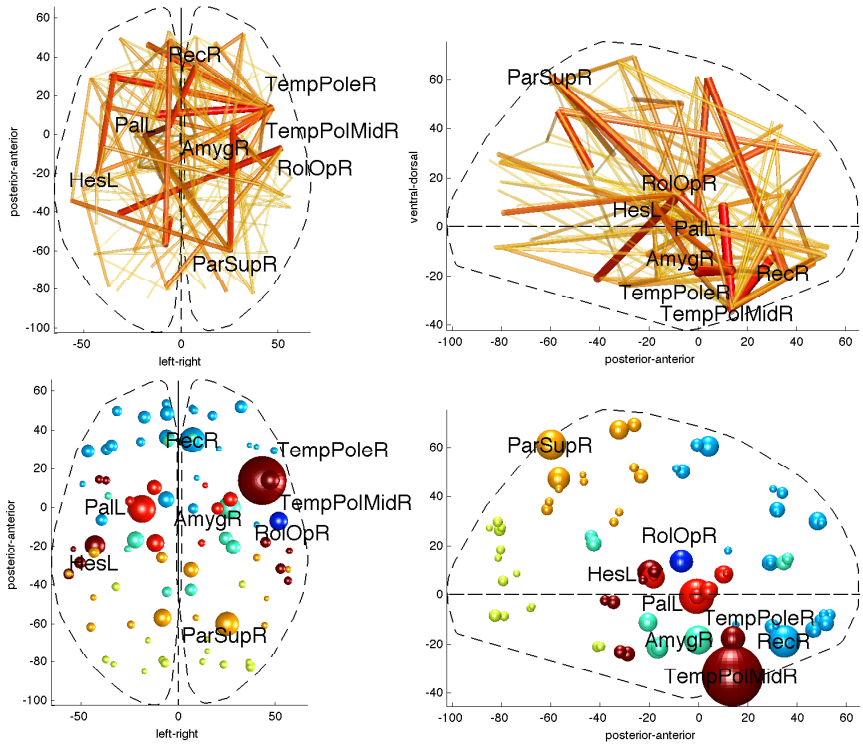

Figure 2: Anatomical illustration of discriminative graphs for MS versus control subjects. In the top row, the size and shade of connections between regions reflects their discriminative weight: stronger hues and larger sizes reflect higher discriminative weight. In the bottom row, the size of each sphere depicting an atlas region is proportional to its regional discriminative weight (sum of the discriminative weights of all connections between this region and the rest of the brain). Colour indicates the lobe where each region is located (dark red = temporal, clear blue = frontal, yellow = parietal, green = occipital, cyan = limbic structures (cingulum, hippocampus and parahippocampal formation, amygdala) and insula, clear red = subcortical grey matter). Name labels are given for the regions with the highest regional discriminative weights (limited to 8 for clarity).

connections with high discriminative weight, both long-range and short-range. More remarkably, the temporal lobe and subcortical grey nuclei contain a few important hubs showing marked changes in connectivity between patients and controls.

The discriminative power of each individual lobe is summarised in Figure 3 (left), with separate plots for within-lobe and between-lobe connections. As can be seen, discriminative connections are predominantly inter-lobe, but intra-lobe connections are equally or more important for temporo-parietal regions. The latter typically correspond to long range pathways in posterior-anterior axis along the periventricular regions. Connections to and from subcortical regions are also particularly discriminative, highlighting the widespread connectivity of these structures.

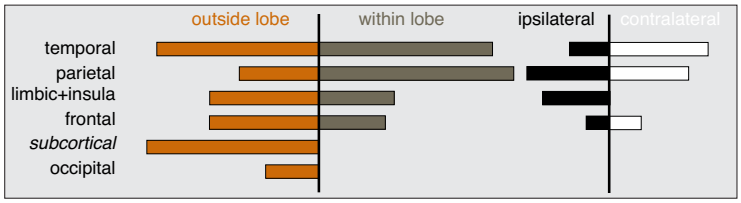

Figure 3: (left graph) Summary of discriminative weights of ROIs by lobe, distinguishing connections that link to other regions outside the lobe from connections that stay within the same lobe. The lobes are ordered from overall most discriminative to overall least discriminative. Limbic structures include cingulum, hippocampus and parahippocampal formation, and amygdala. (right graph) Further subdivision of within-lobe connections into ipsilateral and contralateral connections.

Because inter-hemispheric connections are likely to rely on the corpus callosum which is a known location for MS lesions (Noseworthy et al., 2000; Rocca et al., 2007; Compston and Coles, 2008), it is of particular interest to separate the discriminative graph into ipsi- and contra-lateral subgraphs (C_I and C_C). Inspection of the discriminative graph in Figure 2 suggests that some connections with contralateral areas may have larger discriminative power (a detailed subdivision is available in Supplementary Figure 3). This is confirmed ($p \ll 0.01$ and generalised $\eta^2 = 0.8$) by a repeated measures ANOVA testing the effect of grouping by subgraphs C_I or C_C on the sum of significant discriminative weights in each cross-validation folds. Nevertheless, it should be noted that there clearly is a large amount of discriminative information in the ipsi-lateral subgraph as well. This implies that the functional connectivity at rest is altered by MS both within and between brain hemispheres, and that both types of changes are reliable indicators of the disease.

Moreover, at detailed look at connections across lobes reveals a subtler picture: When the discriminative weights of each lobe are divided into ipsi- and contra-lateral parts (Figure 3, right part)) the temporal lobe shows the most predictive differences for inter-hemispheric connections, whereas limbic structures (cingulum, hippocampus and parahippocampal formation, and amygdala) and the insula only show alterations in intra-hemispheric functional connectivity. Parietal and frontal lobes seem to have an equal balance of discriminative weight between inter- and intra-hemispheric connections.

Finally, it is also important to distinguish between increases and decreases in connectivity. When examining the whole network, we found that discrimination

is mostly driven by connections that are on average stronger in controls, suggesting a characteristic reduction of functional connectivity in patients. However, there is a set of ROIs where some connections with other areas show increased connectivity in patients. Figure 4 shows a division of the discriminative graph into a subnetwork with increased connectivity in patients with respect to controls (C_+) and vice-versa (C_-). It is apparent that the regions involved in C_+ form a network whose main connections link the thalamus to medial and anterior temporal pole, mainly contralaterally (with stronger effects for the right hippocampus, right amygdala, and bilateral temporal poles). Connections are also heightened between the right amygdala, right hippocampus, and right temporal pole. Several connections to and from the left parahippocampal regions are also stronger in this network. Supplementary Figure 2 shows the relative discriminative weight of some of these connections. These increases of connectivity in MS patients therefore appear much more circumscribed than decreases which are observed for long-range pathways both within and across hemispheres.

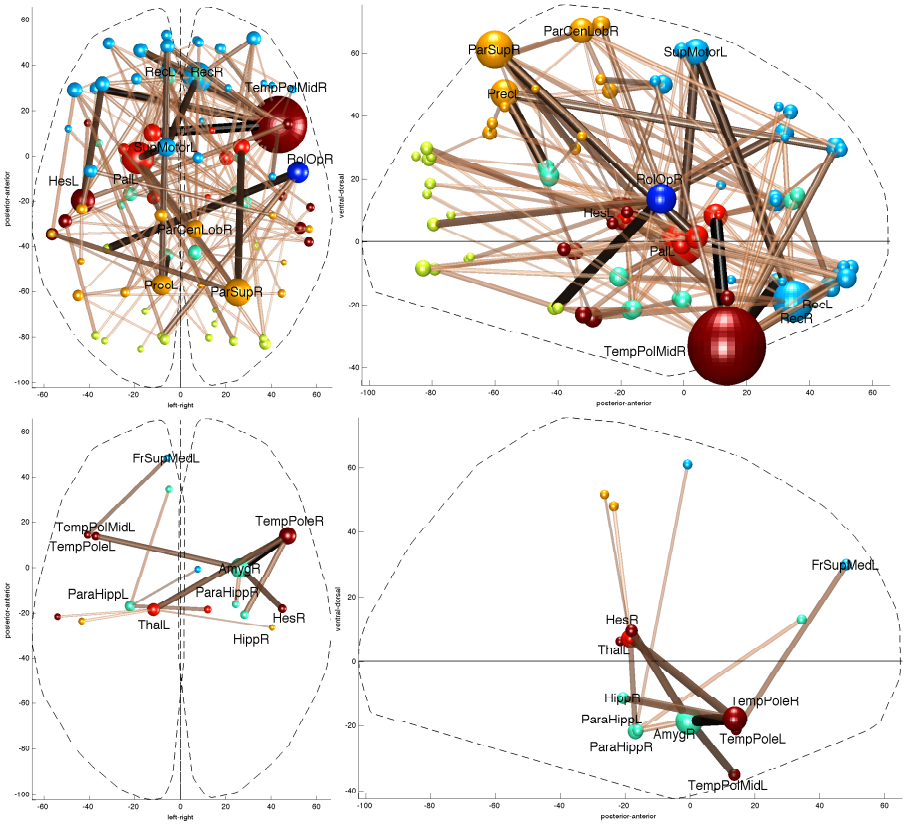

Figure 4: (top) Subnetwork where patients have on average weaker connectivity than controls (C_-). (bottom) Subnetwork where patients have on average stronger connectivity than controls (C_+). The size and shade of connections between regions reflects their discriminative weight: stronger hues and larger sizes reflect higher discriminative weight. The size of spheres for atlas regions is proportional to its regional discriminative weight Colour indicates the lobe each region is part of (see Figure 2 for the colour coding).

2.3. Connections outside the default-mode network are also informative

Studies have highlighted alterations to the DMN (Buckner et al., 2008) associated with multiple sclerosis (Roosendaal et al., 2010; Bonavita et al., 2011). To investigate this effect more specifically in our data, a subnetwork of the whole-brain graph comprising regions that are part of the DMN was defined (based on the work of Buckner et al. (2008), and including the ventral and medial prefrontal cortex, the posterior cingulate and retrosplenial cortex, inferior parietal lobule, lateral temporal cortex, and hippocampal formation. Details are in Supplementary Table 3. The discriminative weight of connections within the default-mode network was tallied separately from the discriminative weight of connections to the outside of the default-mode network.

Results are summarized in Figure 5, clearly showing that discriminative changes do not only affect connections between DMN regions, but also connections between DMN regions and the rest of the brain. In fact, more discriminative information is contained in regions that are not part of the DMN, highligthing the interest of examining whole-brain networks. Remarkably, however, the region with the highest discriminative weight, the right middle temporal pole, is part of the default mode network. Moreover, several DMN regions, such as the left precuneus, the bilateral superior frontal orbital cortex, and the right anterior and posterior cingulate cortex, exhibit more discriminative connections to and from the DMN than to and from the rest of the brain. This is consistent with the existence of a specific functional architecture of the DMN that is disrupted by MS pathology.

3. Discussion

The present study shows that a multivariate approach based on predictive modelling of brain connectivity at rest allows a reliable differentiation of minimally-disabled multiple sclerosis patients and healthy control subjects. Our results do not only confirm that functional changes affecting widespread (cortical and subcortical) networks are a prominent feature of MS brain pathology (Miller et al., 2003) but also show that these alterations can be reliably and sensitively measured using functional MRI of resting state, and furthermore be used to classify disease state in individual subjects. Our method is based on an established technique of brain decoding using wavelet decomposition of resting state time courses (Richiardi et al., 2011; Eryilmaz et al., 2011), previously applied to study cognitive and emotional states in normal conditions, but adapted here to assess pathological states.

Used rigorously, classifiers in a pattern recognition approach provide very powerful tools to explore high-dimensional data and to capture consistent but unknown features, without limiting the findings to specific hypotheses. Our results take into account the full high-dimensional data consisting of 90×90 connections, but the discriminative graphs showing the distinctive functional connections are readily interpretable and the results can even be summarised by two principal measures: the reduced connectivity index (RCI) and the increased connectivity index (ICI), which reflect the main characteristics of connectivity alterations. Furthermore, by using a leave-one-subject-out cross-validation technique, the results have shown the applicability of our method to single subjects. With important caveats, the performance obtained with the proposed method

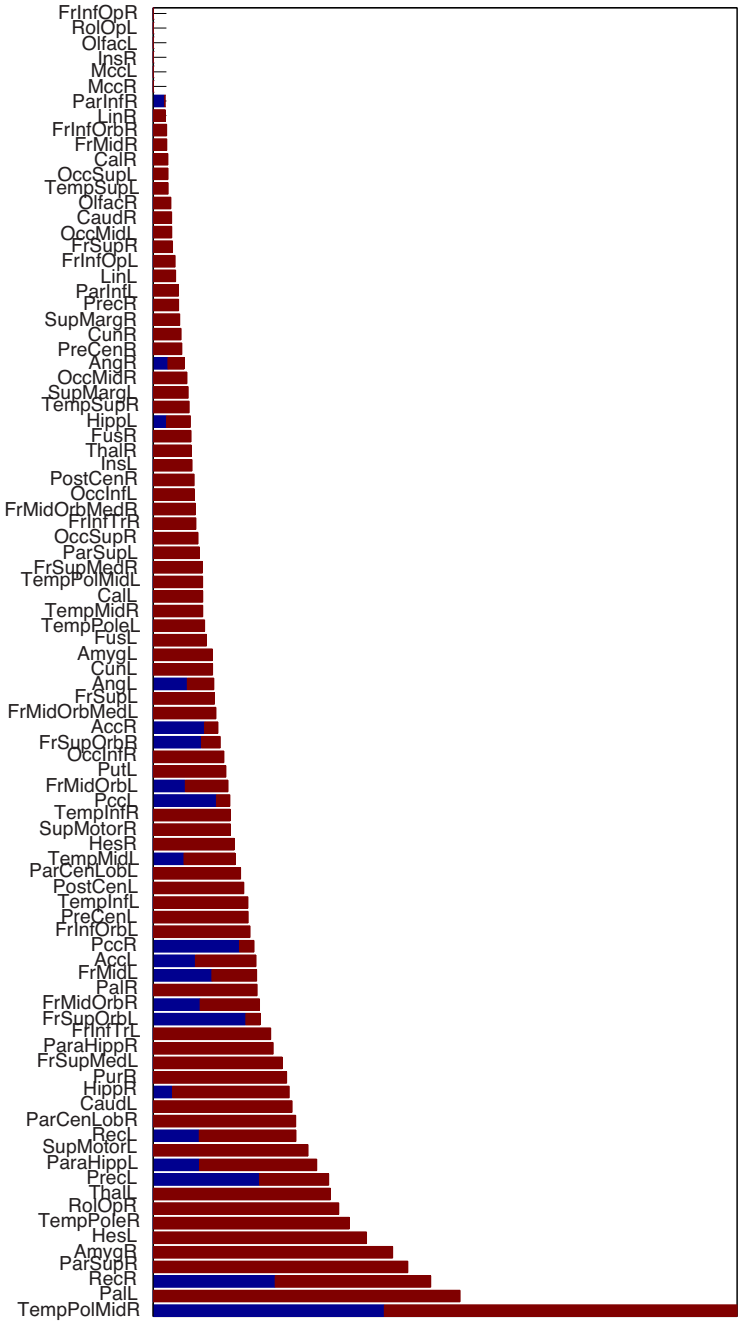

Figure 5: Regional discriminative weights divided into connections within (blue, close to axis) and outside (red, away from axis) the DMN.

can be compared with the results of Weygandt et al. (2011), based on a searchlight approach to structural T2-weighted images. In particular, their larger study population is in generally worse condition (longer average disease duration, larger EDSS range (maximum: 7)) and their analysis uses the cerebellum as well. While the best performance (96% leave-one-out balanced accuracy) is obtained using hand-segmented lesion masks, the analysis of normal appearing gray matter yields up to 82% balanced accuracy, and normal appearing white matter yields up to 91% accuracy. Our results, at 84% balanced accuracy, can therefore be considered encouraging since no cerebellum is used in our study, and the population is minimally disabled. Furthermore, subtle white matter alterations, to which our technique is sensitive, seem to be in and of themselves discriminative, which hints at possible future gains in accuracy by refining our method. However, and despite their statistical significance, our current sensitivity and specificity figures must still be taken with caution because of our limited sample size. MS is a heterogeneous disease, and our leave-one-out results offer only limited evidence of generalisation ability to a separate cohort.

Many other analyses of resting state in neurological diseases concentrated on the default mode network (DMN), or focused on a small number of regions, for example by using univariate methods to compare the goodness of fit of patients and controls to a standard DMN template (Greicius et al., 2004), or by measuring the cross-correlation coefficient of activity over time for a single region (Li et al., 2002). In MS, some studies (Lowe et al., 2008) explored functional connectivity only to and from motor areas and did not find significant whole-group difference between minimally-disabled MS patients and healthy controls. Moreover, many of the few studies addressing resting state alterations in MS concentrated only on the DMN (Rocca et al., 2010; Bonavita et al., 2011). However MS lesions are not restricted to the DMN. Our results show that the connections within DMN regions are affected, but do not represent the only nor the most common ones contributing to correct classification. The major advantages of our multivariate approach, taking into account connectivity across the entire brain, include a greater versatility and a higher sensitivity, two crucial features for discriminating different conditions and studying early stages of pathology. Whole-brain analysis using ICA in MS has indeed been reported to bring out significant differences between groups in various brain networks apart from the DMN Roosendaal et al. (2010). Additionally, the good performance of using multivariate methods with whole-brain functional data to derive imaging markers has also been reported in other pathologies, for example depression (see e.g. Greicius et al. (2007); Craddock et al. (2009)) or Alzheimer's disease (see e.g. Buckner et al. (2009); Chen et al. (2011)).

Overall, our data indicate that only about 4% of the total possible connections considered in our study (between the 90 ROIs distributed over the entire cortex and subcortical nuclei) are discriminative between minimally disabled MS patients and healthy controls. Thus, the large majority (i.e., the remaining 96%) of functional connections have non-significant discriminative weights. However, these 4% still represent numerous (161) connectivity pairs. Although there is no single pathognomonic path affected by MS (consistent with widely distributed lesions (Compston and Coles, 2008; Polman et al., 2011)), these altered connections are not uniformly distributed across the brain and specific patterns are visible. Below, we discuss the possible significance of these changes.

3.1. Topology of the discriminative connections

The discriminative connections between all ROIs considered were located throughout the brain, including in particular the temporal lobes (with a predominance for the right temporal pole), the superior parietal lobes, as well as the frontal lobes and some limbic structures, plus several structures among subcortical grey nuclei. Strikingly, in contrast, the connections concerning the occipital lobe had very low discriminative weight, although clinically MS often presents with visual disturbances (Compston and Coles, 2008; Noseworthy et al., 2000). However, the latter are typically related to an early affection of optic tracts (Ciccarelli et al., 2005; Reich et al., 2009; Dineen et al., 2009), which was not specifically investigated here.

The discriminative connections were mostly associated with long-range pathways presumably grouped around the ventricles for intra-parietal and intra-temporal pairs, or centred on inter-hemispheric pathways for parieto-parietal and temporo-temporal connections. Frontal and limbic connections were also affected but to a lesser extent. This observation converges with the preferential location of MS lesions in areas of dense venular distributions, i.e. around the lateral ventricles, and at the cortico-subcortical junction (Compston and Coles, 2008). In addition, the connectivity of deep grey matter nuclei (thalamus and basal ganglia) was also markedly affected, which is consistent with the fact that these subcortical nuclei both receive and project to large parts of the neocortex, and that many of these projections also travel in periventricular white matter (e.g. thalamic radiations).

Notably, among connections with significant discriminative weight across the whole brain, we found that inter-hemispheric connections are more discriminative than intra-hemispheric connections, even though the latter still make an important contribution to discriminative power. This finding is compatible with the well-known preferential affection of the corpus callosum in MS (Gean-Marton et al., 1991; Evangelou et al., 2000; Mesaros et al., 2009; Rocca et al., 2010; Yaldizli et al., 2011) and presumably reflects in part the concentration of all inter-hemispheric connections at a relatively small circumscribed location in the brain. Our results therefore add to previous studies reporting a decreased inter-hemispheric functional connectivity at rest in MS patients (Cover et al., 2006). However, out data also go beyond these studies by demonstrating that such decreases are not specific to inter-hemispheric connections, since most of the functional connectivities with a significant discriminative weight are decreased in patients, both within and between the two hemispheres. As a particular case, we found that inter-hemispheric connections in limbic structures (cingulum, hippocampus and parahippocampal formation, and amygdala) and the insula provide no discriminating information about patients and controls. Taken together, these findings highlight the importance of considering intra-hemispheric connections when analysing functional connectivity in MS, even in resting-state conditions. We cannot exclude the possibility, however, that the relatively high significance of intra-hemispheric pathways (compared to inter-hemispheric pathways) may reflect the minimal disability in our patients, given the known association between callosal atrophy and disease progression (Pelletier et al., 2001).

Several of the relatively most discriminative connections were centred around the right temporal pole – including left caudate to right middle temporal pole,

right amygdala to right temporal pole, left inferior frontal orbital to right middle temporal pole, and left superior frontal orbital to right middle temporal pole. However, it must be kept in mind that these pairs represent only the top of 161 discriminative connections that all together are responsible for multivariate pattern classification, and that none of these connections is significantly discriminative on its own. Looking for a more synthetic view, a region that is part of several discriminative connection pairs becomes a discriminative region itself. Under this measure, the most discriminative regions were located in the anterior right temporal lobe, but also in the bilateral superior parietal lobes, orbitofrontal cortex (gyrus rectus), left globus pallidus, and right amygdala. An alteration of the underlying structural connectivity (due to white-matter injury) is likely to account for the important impact of MS on a few specific regions such as the temporal pole or pallidum, as these regions are known to constitute strong hubs in brain connectivity (Olson et al., 2007; Haber and Knutson, 2010). In particular, the temporal poles are densely connected to orbito-frontal cortex (via the uncinate fasciculus), amygdala, temporal and occipital ventral regions (via the inferior longitudinal fasciculus), as well as the temporo-parietal junction, and as such constitute high-level associative cortical areas integrating deeply processed information from various parts of the brain (Olson et al., 2007). By being somewhat at the "top of processing hierarchy", these temporal areas might reflect a common impact of disrupted connectivity in widespread pathways throughout the brain.

We also note that many functional connections highlighted by the present approach may not necessarily imply the existence (or damage to) direct structural connections. In fact, coherent activity between distant areas might be subserved by either direct white-matter pathways or more global synchronization processes involving other nodes in a common networks and/or diffuse projections from subcortical (e.g. brainstem) structures (see Golanov and Reis (1996) for an example in the rat). These more global influences might account for connections found across non-homologous areas between the two hemispheres. While our methodology cannot distinguish between structural and non-structural sources of functional connectivity, it is likely to gain higher sensitivity by measuring the impact of diffuse lesions that may affect both types of connections.

3.2. Decreased and increased connectivity in MS patients

Most of the significant connectivity changes reflected decreases in patients compared to controls, consistent with an impaired functional coupling between distant brain areas due the presence of MS lesions. However there were also a few connections showing increased strength in MS compared to controls. These connections were found in a specific subnetwork, roughly consisting of bilateral and inter-hemispheric connections around the thalami, medial temporal areas (para-hippocampal gyrus, amygdalae), and temporal pole. An increase in low-frequency activations (not connectivity) in the thalamus, insula, and superior temporal gyrus has previously been reported in MS (Liu et al., 2011) and interpreted as compensatory plasticity. Here, however, we did not find changes in insula connections allowing a reliable group discrimination, but the insula is also known to be connected to the temporal pole and amygdala (Augustine, 1996).

Note that our method is sensitive to both reduced and increased connectivity without any a priori. Increased connectivity (reflected in the ICI values) by itself

is however not a discriminating feature between patients and controls, because information about increased connectivity is significant only together with the concomitant reduction in connectivity (reflected in the RCI). Nevertheless, in our data, the strongest distinction between subjects and controls is provided by the RCI, and considering only the sum of correlations for reduced connections (projection on the RCI axis of Figure 1) still shows a reliable separation between patients and controls. This may suggest that the phenomena of decreased and increased connectivity in distinct subnetworks in MS are likely to result from concomitant but distinct factors.

The meaning of increased connectivities is not completely clear. Along with the decreased connectivities, these might reflect functional reorganisation to cope with pathological damage, in keeping with results from several imaging studies in MS (Reddy et al., 2000a; Morgen et al., 2004; Mainero et al., 2004; Morgen et al., 2007; Trapp et al., 1998; Cifelli and Matthews, 2002; Rocca and Filippi, 2007; Hawellek et al., 2011). Compensatory activation is often considered as a process arising at early stages, which tends to be lost with disease progression (Bonavita et al., 2011; Roosendaal et al., 2010). Congruent with this hypothesis, the positive nRCI correlation found with lesion loads (see Section 2.1) seems to suggest that connectivity in the C_- subnetwork is increased to cope with lesions. However, our findings of increased connectivity in the C_+ subnetwork and increasing connectivity with lesion load in C_- might be specific to minimally-disabled MS patients, a possibility that will require further testing in additional patients with more severe disease.

Note that in our study, this C_+ subnetwork predominantly concerns medio-temporal and orbito-frontal regions, normally associated with emotional processing (Kensinger and Schacter, 2008), and could therefore possibly reflect latent affective disturbances often associated with MS (Minden and Schiffer, 1990; Compston and Coles, 2008) and/or higher stress levels in patients during an MRI session (Muehlhan et al., 2011). Alternatively, we cannot exclude that the observed increases in connectivity might partly reflect stronger coherence at low frequencies due to an "idling" state of some networks at rest (Richiardi et al., 2011), subsequent to disconnection lesions in patients. Again, additional studies in patients with a broader range of MS severity will be necessary to disentangle these hypotheses.

3.3. Discriminative connections inside and outside the default mode network

Our results confirm that the default mode network (DMN) comprises many discriminative connections that are affected by MS (Roosendaal et al., 2010; Rocca et al., 2010; Bonavita et al., 2011), but they also highlight a large number of additional discriminative connections outside the DMN. Studies of resting-state brain activity often focus on the default-mode network because it forms a well-defined set of regions that is observed very reproducibly under different acquisition paradigms. In fact, the most discriminative ROIs in our analysis, the right temporal pole, is also part of the DMN and "consistently observed across approaches" (Buckner et al., 2008). We also found an important role for the precuneus, another core region of the DMN. In addition, we found weaker connectivity in the anterior cingulate cortex of MS patients, as reported in a previous study of resting state in MS (Bonavita et al., 2011), but an opposite effect in the posterior cingulate cortex (decreased rather than increased connectivity in patients). Nevertheless, as clearly shown in figure 5, many other regions

that are not part of the DMN made a crucial contribution to the discrimination between patients and controls. Therefore, we conclude that resting-state data analysis in MS (and other neurological conditions) should certainly comprise default-mode network regions, but need not be restricted to them.

3.4. Altered connectivity and grey matter changes

The analysis of functional connectivity is based on temporal correlations of activity between grey matter ROIs. In case of decreased connectivity, it is in principle not possible to differentiate between desynchronisation due to loss of white-matter pathways or grey-matter pathology in one or more of the connected ROIs. Thus, functional connectivity is sensitive to both white-matter and grey-matter pathology, and permits the investigation of both aspects of MS.

In general, MS lesions are predominantly located in white matter, and therefore mainly affect axonal conduction. However, damage to cortical grey matter is also increasingly recognized (Bö et al., 2006; Prinster et al., 2006; Barkhof et al., 2009). Interestingly, our results for regional discriminative weights in different lobes show convergent patterns with what is known from anatomical studies on focal grey matter lesions (Filippi and Agosta, 2010). For instance, we found that the thalamus is involved in a high number of discriminative connections at rest. The thalamus is known to be a site of preferential atrophy in MS (Cifelli et al., 2002; Wylezinska et al., 2003; Audoin et al., 2006), possibly resulting in decreased perfusion (Rashid et al., 2004). In addition, the connections to and from several deep nuclei such as the globus pallidus, caudate, and amygdala, were also discriminating between patients and controls. Early and frequent lesions in the thalamus and caudate as well as in the putamen, globus pallidus, or amygdalae have been recently pointed out (Vercellino et al., 2009), and these regions exhibit a rapid atrophy following the first clinical event (Audoin et al., 2010). Deep gray matter regions (caudate, lentiform) have also been reported as discriminative using multivariate predictive modelling on structural T2-weighted data (Weygandt et al., 2011). Overall, the importance of deep grey matter and subcortical areas is likely to reflect their key position as regions of convergence and divergence of many cortico-cortical loops.

Likewise, some temporal regions (with high regional discriminative weights in our data) have also been found to show a particularly early occurrence of grey matter atrophy and cortical thinning, even after less than 3 years disease duration (Sailer et al., 2003). Recent multivariate predictive modelling results on structural images also report the relative high importance of the superior temporal gyrus and middle temporal gyrus (among others) in distinguishing early from late MS patients (Bendfeldt et al., 2012). The marked asymmetry in the right compared to the left temporal pole is unexplained, although this may reflect some characteristic of our patient sample, or a predominant recruitment of right-hemispheric areas in mental and affective processes associated with resting state (for example Yan et al. (2009) report significantly higher right-intrahemispheric connectivity at rest between a set of regions including the middle temporal gyrus). However, a mid-sagittal asymmetry of gray matter damage has also been reported together with decreased gray matter volume in the left fronto-temporal cortex in RRMS patients (Prinster et al., 2006).

3.5. Limitations and outlook

Beyond information on disease pathophysiology and possible correlations with clinical symptoms, our approach offers a new tool to assess disease probability. Our results demonstrate very good classification accuracy (sensitivity 82%, specificity 86%) for the differentiation of clinically definite MS patients with minimal disability (median EDSS 2) from healthy controls. These data reveal that rich information can be extracted from 8 minutes of resting-state fMRI. Given its complementarity with other diagnostic modalities, future studies should further investigate the sensitivity of this approach for patients with suspected MS or clinically isolated syndromes, and explore its use for monitoring evolution or treatment effects. A particular interest will be the investigation of the link between connectivity alterations and clinically-relevant scales, as interesting links with cognitive performance have been found by other authors (Hawellek et al., 2011). Additionally, spatial relationship between lesion locations and connectivity alterations at the single subject level would be of great interest in order to improve result interpretation with respect to specific attack types.

However, the interpretation of such results must be done with care, as functional connectivity, by nature, reflects not only monosynaptic anatomical connections, but also functional entities in multirelay connections. Moreover, as a purely data-driven method, the performance of our classifier depends on the amount of data available, and is sensitive to artifactual influences or uncontrolled factors, e.g. patient movement, which may prevent its use due to degradation or contamination of the BOLD signal. The movement correction and robust statistics techniques employed here can help mitigate these problems, but it is clear that this method will not be amenable to some patients (such as those exhibiting large tremors). Because deep grey matter seems to play an important role in discrimination results, several combinations of MRI head coils, scanner field strengths, and imaging sequences may not be suitable if they fail to yield signal with sufficient contrast-to-noise ratio in these regions, or present too much susceptibility artifacts (as amygdala and orbito-frontal regions).

Inter-scanner reliability is another topic where more work is needed. The use of relatively large atlas regions in our study, combined with taking the temporal mean of regions which constitutes aggressive spatial smoothing, lead us to believe the method could be used in a multi-centric setting. Indeed, inter-scanner reproducibility of BOLD fMRI activation results is known to increase with region-based measure rather than voxel-based measures (Demirci et al., 2008), and more so when regions are large and smoothed (Friedman et al., 2008). In a recent functional connectivity study of MS using group statistics, 8 different sites with different manufacturers, models, and sequences could lead to statistically significant results concerning the difference in functional connectivity of MS patients, simply by including acquisition centre as a model factor (Valsasina et al., 2011). However, a serious study of predictive modelling of connectivity across sites remains to be undertaken.

In sum, our study shows that a multivariate approach of predictive modelling allows a discrimination of brain connectivity at rest between minimally disabled MS patients and healthy control subjects. The model prediction was based on a large number of altered connections between grey matter areas, involving temporal, frontal, parietal, and subcortical grey matter regions. These

connections were generally weaker for the patients, concerned both inter- and intra-hemispheric connectivity, and extended beyond regions of the default network to affect a large number of connections between other brain regions. This study is only the first, but necessary step towards novel resting-state based imaging marker of MS, and its results will have to be confirmed and refined with larger patient samples, including more advanced stages, and other neurodegenerative or inflammatory pathologies, in order to obtain a prognosis model. Validation with an second, separate cohort of patients would be very beneficial, in particular because MS has a very heterogeneous presentation.

Funding

This work was supported in part by Merck Serono (Merck Serono-EPFL Research Alliance Award), in part by the Swiss National Science Foundation (grant number PP00P2-123438); the Société Académique de Genève (FOREMANE fund); the Swiss Society for Multiple Sclerosis; the Center for Biomedical Imaging (CIBM) of the Geneva and Lausanne Universities, EPFL, and the Leenaards and Louis-Jeantet foundations; and the US National Science Foundation (grant number NSF PHY05-51164).

Acknowledgements

The authors wish to thank Prof. E.W. Radue for organising the tracing of the MS lesions at the Medical Image Analysis Center of the University Hospital Basel. We also wish to thank Prof R. Meuli for the scanning protocol, and Michel Dreano for his comments and discussion leading up to this paper.

References

Achard, S., Salvador, R., Whitcher, B., Suckling, J., Bullmore, E., Jan. 2006. A resilient, low-frequency, small-world human brain functional network with highly connected association cortical hubs. The Journal of Neuroscience 26 (1), 63–72.

Alemán-Gómez, Y., Melie-García, L., Valdés-Hernandez, P., June 2006. IBASPM: Toolbox for automatic parcellation of brain structures. In: Proc. 12th Annual Meeting of the Organization for Human Brain Mapping. Florence, Italy.

Ashburner, J., Friston, K. J., Jul 2005. Unified segmentation. Neuroimage 26 (3), 839–851.

Audoin, B., Davies, G. R., Finisku, L., Chard, D. T., Thompson, A. J., Miller, D. H., 2006. Localization of grey matter atrophy in early rrms. Journal of Neurology 253 (11), 1495–1501.

Audoin, B., Zaaraoui, W., Reuter, F., Rico, A., Malikova, I., Confort-Gouny, S., Cozzone, P. J., Pelletier, J., Ranjeva, J.-P., Jun 2010. Atrophy mainly affects the limbic system and the deep grey matter at the first stage of multiple sclerosis. J Neurol Neurosurg Psychiatry 81 (6), 690–695.

Augustine, J. R., Oct 1996. Circuitry and functional aspects of the insular lobe in primates including humans. Brain Res Brain Res Rev 22 (3), 229–244.

Barkhof, F., 2002. The clinico-radiological paradox in multiple sclerosis revisited. Current Opinion in Neurology 15 (3), 239–245.

Barkhof, F., Calabresi, P. A., Miller, D. H., Reingold, S. C., May 2009. Imaging outcomes for neuroprotection and repair in multiple sclerosis trials. Nature Reviews Neurology 5 (5), 256–266.

Barkhof, F., Filippi, M., Apr. 2009. Multiple sclerosis: MRI–the perfect surrogate marker for multiple sclerosis? Nature Reviews Neurology 5 (4), 182–183.

Bendfeldt, K., Klöppel, S., Nichols, T. E., Smieskova, R., Kuster, P., Traud, S., Mueller-Lenke, N., Naegelin, Y., Kappos, L., Radue, E.-W., Borgwardt, S. J., Mar. 2012. Multivariate pattern classification of gray matter pathology in multiple sclerosis. NeuroImage 60 (1), 400–408.

Biswal, B., Yetkin, F., Haughton, V., Hyde, J., 1995. Functional connectivity in the motor cortex of resting human brain using echo-planar MRI. Magnetic Resonance in Medicine 34 (4), 537–541.

Bonavita, S., Gallo, A., Sacco, R., Corte, M. D., Bisecco, A., Docimo, R., Lavorgna, L., Corbo, D., Costanzo, A. D., Tortora, F., Cirillo, M., Esposito, F., Tedeschi, G., 2011. Distributed changes in default-mode resting-state connectivity in multiple sclerosis. Multiple Sclerosis Journal 17 (4), 411–422.

Breiman, L., Aug. 1996. Bagging predictors. Machine Learning 24 (2), 123–140.

Buckner, R., Andrews-Hanna, J., Schacter, D., 2008. The brain's default network: Anatomy, function, and relevance to disease. Annals of the New York Academy of Sciences 1124, 1–38.

Buckner, R. L., Sepulcre, J., Talukdar, T., Krienen, F. M., Liu, H., Hedden, T., Andrews-Hanna, J. R., Sperling, R. A., Johnson, K. A., 2009. Cortical hubs revealed by intrinsic functional connectivity: Mapping, assessment of stability, and relation to alzheimer's disease. The Journal of Neuroscience 29 (6), 1860–1873.

Budde, M. D., Xie, M., Cross, A. H., Song, S.-K., 2009. Axial diffusivity is the primary correlate of axonal injury in the experimental autoimmune encephalomyelitis spinal cord: A quantitative pixelwise analysis. The Journal of Neuroscience 29 (9), 2805–2813.

Bö, L., Geurts, J., Mörk, S., Van Der Valk, P., 2006. Grey matter pathology in multiple sclerosis. Acta Neurologica Scandinavica 113 (SUPPL. 183), 48–50.

Cader, S., Cifelli, A., Abu-Omar, Y., Palace, J., Matthews, P. M., Feb 2006. Reduced brain functional reserve and altered functional connectivity in patients with multiple sclerosis. Brain 129 (Pt 2), 527–537.

Chen, G., Ward, B. D., Xie, C., Li, W., Wu, Z., Jones, J. L., Franczak, M., Antuono, P., Li, S.-J., Apr 2011. Classification of alzheimer disease, mild cognitive impairment, and normal cognitive status with large-scale network analysis based on resting-state functional mr imaging. Radiology 259 (1), 213–221.

Ciccarelli, O., Toosy, A. T., Hickman, S. J., Parker, G. J. M., Wheeler-Kingshott, C. A. M., Miller, D. H., Thompson, A. J., Jul 2005. Optic radiation changes after optic neuritis detected by tractography-based group mapping. Hum Brain Mapp 25 (3), 308–316.

Cifelli, A., Arridge, M., Jezzard, P., Esiri, M. M., Palace, J., Matthews, P. M., 2002. Thalamic neurodegeneration in multiple sclerosis. Annals of Neurology 52 (5), 650–653.

Cifelli, A., Matthews, P. M., May 2002. Cerebral plasticity in multiple sclerosis: insights from fMRI. Mult Scler 8 (3), 193–199.

Compston, A., Coles, A., Oct 2008. Multiple sclerosis. Lancet 372 (9648), 1502–1517.

Cover, K. S., Vrenken, H., Geurts, J. J. G., van Oosten, B. W., Jelles, B., Polman, C. H., Stam, C. J., van Dijk, B. W., Feb 2006. Multiple sclerosis patients show a highly significant decrease in alpha band interhemispheric synchronization measured using meg. Neuroimage 29 (3), 783–788.

Craddock, R. C., Holtzheimer, P. E., Hu, X. P., Mayberg, H. S., Dec 2009. Disease state prediction from resting state functional connectivity. Magn Reson Med 62 (6), 1619–1628.

Demirci, O., Clark, V. P., Magnotta, V. A., Andreasen, N. C., Lauriello, J., Kiehl, K. A., Pearlson, G. D., Calhoun, V. D., Sep 2008. A review of challenges in the use of fmri for disease classification / characterization and a projection pursuit application from multi-site fmri schizophrenia study. Brain Imaging Behav 2 (3), 147–226.

Dineen, R. A., Vilisaar, J., Hlinka, J., Bradshaw, C. M., Morgan, P. S., Constantinescu, C. S., Auer, D. P., Jan 2009. Disconnection as a mechanism for cognitive dysfunction in multiple sclerosis. Brain 132 (Pt 1), 239–249.

Eryilmaz, H., Ville, D. V. D., Schwartz, S., Vuilleumier, P., Feb 2011. Impact of transient emotions on functional connectivity during subsequent resting state: a wavelet correlation approach. Neuroimage 54 (3), 2481–2491.

Ethofer, T., Van De Ville, D., Scherer, K., Vuilleumier, P., June 23, 2009. Decoding of emotional information in voice-sensitive cortices. Current Biology 19 (12), 1028–1033.

Evangelou, N., Esiri, M., Smith, S., Palace, J., Matthews, P., 2000. Quantitative pathological evidence for axonal loss in normal appearing white matter in multiple sclerosis. Annals of Neurology 47 (3), 391–395, cited By (since 1996) 238.

Filippi, M., Agosta, F., Apr 2010. Imaging biomarkers in multiple sclerosis. J Magn Reson Imaging 31 (4), 770–788.

Fox, M. D., Greicius, M., 2010. Clinical applications of resting state functional connectivity. Front Syst Neurosci 4, 19.

Fox, M. D., Raichle, M. E., Sep. 2007. Spontaneous fluctuations in brain activity observed with functional magnetic resonance imaging. Nat Rev Neurosci 8 (9), 700–711.

Fransson, P., Marrelec, G., Sep 2008. The precuneus/posterior cingulate cortex plays a pivotal role in the default mode network: Evidence from a partial correlation network analysis. Neuroimage 42 (3), 1178–1184.

Friedman, J., Hastie, T., Tibshirani, R., 2000. Additive logistic regression: A statistical view of boosting. Annals of Statistics 28 (2), 337–407.

Friedman, L., Stern, H., Brown, G., Mathalon, D., Turner, J., Glover, G., Gollub, R., Lauriello, J., Lim, K., Cannon, T., Greve, D., Bockholt, H., Belger, A., Mueller, B., Doty, M., He, J., Wells, W., Smyth, P., Pieper, S., Kim, S., Kubicki, M., Vangel, M., Potkin, S., 2008. Test-retest and between-site reliability in a multicenter fmri study. Human Brain Mapping 29 (8), 958–972.

Friston, K., Williams, S., Howard, R., Frackowiak, R., Turner, R., 1996. Movement-related effects in fMRI time-series. Magnetic Resonance in Medicine 35 (3), 346–355.

Fu, L., Matthews, P. M., De Stefano, N., Worsley, K. J., Narayanan, S., Francis, G. S., Antel, J. P., Wolfson, C., Arnold, D. L., Jan 1998. Imaging axonal damage of normal-appearing white matter in multiple sclerosis. Brain 121 (Pt 1), 103–113.

Gama, J., Jun. 2004. Functional trees. Machine Learning 55 (3), 219–250.

Gean-Marton, A., Vezina, L., Marton, K., Stimac, G., Peyster, R., Taveras, J., Davis, K., 1991. Abnormal corpus callosum: A sensitive and specific indicator of multiple sclerosis. Radiology 180 (1), 215–221.

Golanov, E. V., Reis, D. J., Aug 1996. Contribution of oxygen-sensitive neurons of the rostral ventrolateral medulla to hypoxic cerebral vasodilatation in the rat. J Physiol 495 (Pt 1), 201–216.

Greicius, M. D., Flores, B. H., Menon, V., Glover, G. H., Solvason, H. B., Kenna, H., Reiss, A. L., Schatzberg, A. F., Sep 2007. Resting-state functional connectivity in major depression: abnormally increased contributions from subgenual cingulate cortex and thalamus. Biol Psychiatry 62 (5), 429–437.

Greicius, M. D., Krasnow, B., Reiss, A. L., Menon, V., Jan. 2003. Functional connectivity in the resting brain: A network analysis of the default mode hypothesis. Proceedings of the National Academy of Sciences of the United States of America 100 (1), 253–258.

Greicius, M. D., Srivastava, G., Reiss, A. L., Menon, V., Mar 2004. Default-mode network activity distinguishes alzheimer's disease from healthy aging: evidence from functional MRI. Proc Natl Acad Sci U S A 101 (13), 4637–4642.

Greicius, M. D., Supekar, K., Menon, V., Dougherty, R. F., Jan 2009. Resting-state functional connectivity reflects structural connectivity in the default mode network. Cereb Cortex 19 (1), 72–78.

Haber, S. N., Knutson, B., Jan 2010. The reward circuit: linking primate anatomy and human imaging. Neuropsychopharmacology 35 (1), 4–26.

Hawellek, D. J., Hipp, J. F., Lewis, C. M., Corbetta, M., Engel, A. K., 2011. Increased functional connectivity indicates the severity of cognitive impairment in multiple sclerosis. Proc National Academy of Sciences of the USA 108 (47), 19066–19071.

Helekar, S. A., Shin, J. C., Mattson, B. J., Bartley, K., Stosic, M., Saldana-King, T., Montague, P. R., Hutton, G. J., 2010. Functional brain network changes associated with maintenance of cognitive function in multiple sclerosis. Front Hum Neurosci 4, 219.

Jacobs, L. D., Beck, R. W., Simon, J. H., Kinkel, R. P., Brownscheidle, C. M., Murray, T. J., Simonian, N. A., Slasor, P. J., Sandrock, A. W., Sep 2000. Intramuscular interferon beta-1a therapy initiated during a first demyelinating event in multiple sclerosis. N Engl J Med 343 (13), 898–904.

Jafri, M. J., Pearlson, G. D., Stevens, M., Calhoun, V. D., Feb 2008. A method for functional network connectivity among spatially independent resting-state components in schizophrenia. Neuroimage 39 (4), 1666–1681.

Jones, D. T., Mateen, F. J., Lucchinetti, C. F., Jack, Jr, C. R., Welker, K. M., Feb 2011. Default mode network disruption secondary to a lesion in the anterior thalamus. Arch Neurol 68 (2), 242–247.

Kamitani, Y., Tong, F., 2005. Decoding the visual and subjective contents of the human brain. Nat. Neurosci. 8, 679–685.

Kappos, L., Freedman, M. S., Polman, C. H., Edan, G., Hartung, H.-P., Miller, D. H., Montalbán, X., Barkhof, F., Radü, E.-W., Bauer, L., Dahms, S., Lanius, V., Pohl, C., Sandbrink, R., B. E. N. E. F. I. T. Study Group, Aug 2007. Effect of early versus delayed interferon beta-1b treatment on disability after a first clinical event suggestive of multiple sclerosis: a 3-year follow-up analysis of the BENEFIT study. Lancet 370 (9585), 389–397.

Kensinger, E. A., Schacter, D. L., 2008. Neural processes supporting young and older adults' emotional memories. Journal of Cognitive Neuroscience 20 (7), 1161–1173.

Kurtzke, J. F., Nov 1983. Rating neurologic impairment in multiple sclerosis: an expanded disability status scale (EDSS). Neurology 33 (11), 1444–1452.

Langs, G., Menze, B. H., Lashkari, D., Golland, P., 2011. Detecting stable distributed patterns of brain activation using gini contrast. NeuroImage 56 (2), 497–507.

Lee, M., Reddy, H., Johansen-Berg, H., Pendlebury, S., Jenkinson, M., Smith, S., Palace, J., Matthews, P. M., May 2000. The motor cortex shows adaptive functional changes to brain injury from multiple sclerosis. Ann Neurol 47 (5), 606–613.

Li, S.-J., Li, Z., Wu, G., Zhang, M.-J., Franczak, M., Antuono, P. G., Oct 2002. Alzheimer disease: evaluation of a functional MR imaging index as a marker. Radiology 225 (1), 253–259.

Lin, X., Tench, C. R., Morgan, P. S., Niepel, G., Constantinescu, C. S., Oct 2005. 'importance sampling' in ms: use of diffusion tensor tractography to quantify pathology related to specific impairment. Journal of the Neurological Sciences 237 (1-2), 13–19.

Liu, Y., Liang, P., Duan, Y., Jia, X., Yu, C., Zhang, M., Wang, F., Zhang, M., Dong, H., Ye, J., Butzkueven, H., Li, K., Feb 2011. Brain plasticity in relapsing-remitting multiple sclerosis: Evidence from resting-state fMRI. J Neurol Sci 304 (1-2), 127–31.

Logothetis, N. K., Jun 2008. What we can do and what we cannot do with fMRI. Nature 453 (7197), 869–878.

Lowe, M. J., Beall, E. B., Sakaie, K. E., Koenig, K. A., Stone, L., Marrie, R. A., Phillips, M. D., Jul 2008. Resting state sensorimotor functional connectivity in multiple sclerosis inversely correlates with transcallosal motor pathway transverse diffusivity. Hum Brain Mapp 29 (7), 818–827.

Lowe, M. J., Mock, B. J., Sorenson, J. A., Feb. 1998. Functional connectivity in single and multislice echoplanar imaging using resting-state fluctuations,. NeuroImage 7 (2), 119–132.

Mainero, C., Caramia, F., Pozzilli, C., Pisani, A., Pestalozza, I., Borriello, G., Bozzao, L., Pantano, P., Mar 2004. fMRI evidence of brain reorganization during attention and memory tasks in multiple sclerosis. Neuroimage 21 (3), 858–867.

Manson, S. C., Palace, J., Frank, J. A., Matthews, P. M., Oct 2006. Loss of interhemispheric inhibition in patients with multiple sclerosis is related to corpus callosum atrophy. Exp Brain Res 174 (4), 728–733.

Manson, S. C., Wegner, C., Filippi, M., Barkhof, F., Beckmann, C., Ciccarelli, O., Stefano, N. D., Enzinger, C., Fazekas, F., Agosta, F., Gass, A., Hirsch, J., Johansen-Berg, H., Kappos, L., Korteweg, T., Polman, C., Mancini, L., Manfredonia, F., Marino, S., Miller, D. H., Montalban, X., Palace, J., Rocca, M., Ropele, S., Rovira, A., Smith, S., Thompson, A., Thornton, J., Yousry, T., Frank, J. A., Matthews, P. M., May 2008. Impairment of movement-associated brain deactivation in multiple sclerosis: further evidence for a functional pathology of interhemispheric neuronal inhibition. Exp Brain Res 187 (1), 25–31.

Mantini, D., Perrucci, M. G., Gratta, C. D., Romani, G. L., Corbetta, M., Aug 2007. Electrophysiological signatures of resting state networks in the human brain. Proc National Academy of Sciences of the USA 104 (32), 13170–13175.

Mesaros, S., Rocca, M. A., Riccitelli, G., Pagani, E., Rovaris, M., Caputo, D., Ghezzi, A., Capra, R., Bertolotto, A., Comi, G., Filippi, M., Aug 2009. Corpus callosum damage and cognitive dysfunction in benign MS. Hum Brain Mapp 30 (8), 2656–2666.

Miller, D. H., Thompson, A. J., Filippi, M., Dec 2003. Magnetic resonance studies of abnormalities in the normal appearing white matter and grey matter in multiple sclerosis. J Neurol 250 (12), 1407–1419.

Minden, S. L., Schiffer, R. B., Jan 1990. Affective disorders in multiple sclerosis. review and recommendations for clinical research. Arch Neurol 47 (1), 98–104.

Morgen, K., Kadom, N., Sawaki, L., Tessitore, A., Ohayon, J., McFarland, H., Frank, J., Martin, R., Cohen, L. G., Nov 2004. Training-dependent plasticity in patients with multiple sclerosis. Brain 127 (Pt 11), 2506–2517.

Morgen, K., Sammer, G., Courtney, S. M., Wolters, T., Melchior, H., Blecker, C. R., Oschmann, P., Kaps, M., Vaitl, D., Sep 2007. Distinct mechanisms of altered brain activation in patients with multiple sclerosis. Neuroimage 37 (3), 937–946.

Mourao-Miranda, J., Bokde, A. L., Born, C., Hampel, H., Stetter, M., Dec. 2005. Classifying brain states and determining the discriminating activation patterns: Support vector machine on functional MRI data. NeuroImage 28 (4), 980–995.

Muehlhan, M., Lueken, U., Wittchen, H.-U., Kirschbaum, C., Feb 2011. The scanner as a stressor: evidence from subjective and neuroendocrine stress parameters in the time course of a functional magnetic resonance imaging session. Int J Psychophysiol 79 (2), 118–126.

Nichols, T. E., Holmes, A. P., 2002. Nonparametric permutation tests for functional neuroimaging: A primer with examples. Human Brain Mapping 15 (1), 1–25.

Noseworthy, J. H., Lucchinetti, C., Rodriguez, M., Weinshenker, B. G., Sep. 2000. Multiple sclerosis. N Engl J Med 343 (13), 938–952.

Olson, I. R., Plotzker, A., Ezzyat, Y., Jul 2007. The enigmatic temporal pole: a review of findings on social and emotional processing. Brain 130 (Pt 7), 1718–1731.

Pelletier, J., Suchet, L., Witjas, T., Habib, M., Guttmann, C. R., Salamon, G., Lyon-Caen, O., Chérif, A. A., Jan 2001. A longitudinal study of callosal atrophy and interhemispheric dysfunction in relapsing-remitting multiple sclerosis. Arch Neurol 58 (1), 105–111.

Polman, C. H., Reingold, S. C., Banwell, B., Clanet, M., Cohen, J. A., Filippi, M., Fujihara, K., Havrdova, E., Hutchinson, M., Kappos, L., Lublin, F. D., Montalban, X., O'Connor, P., Sandberg-Wollheim, M., Thompson, A. J., Waubant, E., Weinshenker, B., Wolinsky, J. S., Feb 2011. Diagnostic criteria for multiple sclerosis: 2010 revisions to the McDonald criteria. Ann Neurol 69 (2), 292–302.

Polman, C. H., Reingold, S. C., Edan, G., Filippi, M., Hartung, H.-P., Kappos, L., Lublin, F. D., Metz, L. M., McFarland, H. F., O'Connor, P. W., Sandberg-Wollheim, M., Thompson, A. J., Weinshenker, B. G., Wolinsky, J. S., 2005. Diagnostic criteria for multiple sclerosis: 2005 revisions to the McDonald criteria. Annals of Neurology 58 (6), 840–846.

Prinster, A., Quarantelli, M., Orefice, G., Lanzillo, R., Brunetti, A., Mollica, C., Salvatore, E., Brescia Morra, V., Coppola, G., Vacca, G., Alfano, B., Salvatore, M., 2006. Grey matter loss in relapsing–remitting multiple sclerosis: A voxel-based morphometry study. NeuroImage 29, 859–867.

Raichle, M. E., MacLeod, A. M., Snyder, A. Z., Powers, W. J., Gusnard, D. A., Shulman, G. L., Jan 2001. A default mode of brain function. Proceedings of the National Academy of Sciences of the United States of America 98 (2), 676–682.

Rashid, W., Parkes, L., Ingle, G., Chard, D., Toosy, A., Altmann, D., Symms, M., Tofts, P., Thompson, A., Miller, D., 2004. Abnormalities of cerebral perfusion in multiple sclerosis. Journal of Neurology, Neurosurgery and Psychiatry 75 (9), 1288–1293.

Ratchford, J. N., Calabresi, P. A., 2008. The diagnosis of MS: White spots and red flags. Neurology 70 (13 Part 2), 1071–1072.

Reddy, H., Narayanan, S., Arnoutelis, R., Jenkinson, M., Antel, J., Matthews, P. M., Arnold, D. L., Nov 2000a. Evidence for adaptive functional changes in the cerebral cortex with axonal injury from multiple sclerosis. Brain 123 (Pt 11), 2314–2320.

Reddy, H., Narayanan, S., Matthews, P. M., Hoge, R. D., Pike, G. B., Duquette, P., Antel, J., Arnold, D. L., Jan 2000b. Relating axonal injury to functional recovery in ms. Neurology 54 (1), 236–239.

Reich, D. S., Smith, S. A., Gordon-Lipkin, E. M., Ozturk, A., Caffo, B. S., Balcer, L. J., Calabresi, P. A., Aug 2009. Damage to the optic radiation in multiple sclerosis is associated with retinal injury and visual disability. Arch Neurol 66 (8), 998–1006.

Richiardi, J., Eryilmaz, H., Schwartz, S., Vuilleumier, P., Van De Ville, D., May 2011. Decoding brain states from fMRI connectivity graphs. NeuroImage (Special Issue on Multivariate Decoding and Brain Reading) 56 (2), 616–626.

Richiardi, J., Van De Ville, D., Riesen, K., Bunke, H., 2010. Vector space embedding of undirected graphs with fixed-cardinality vertex sequences for classification. In: Proc. 20th Int. Conf. on Pattern Recognition (ICPR). pp. 902–905.

Rocca, M. A., Filippi, M., Apr 2007. Functional MRI in multiple sclerosis. J Neuroimaging 17 Suppl 1, 36S–41S.

Rocca, M. A., Pagani, E., Absinta, M., Valsasina, P., Falini, A., Scotti, G., Comi, G., Filippi, M., Dec 2007. Altered functional and structural connectivities in patients with MS: a 3-T study. Neurology 69 (23), 2136–2145.

Rocca, M. A., Valsasina, P., Absinta, M., Riccitelli, G., Rodegher, M. E., Misci, P., Rossi, P., Falini, A., Comi, G., Filippi, M., Apr 2010. Default-mode network dysfunction and cognitive impairment in progressive MS. Neurology 74 (16), 1252–1259.

Rolak, L. A., Fleming, J. O., March 2007. The differential diagnosis of multiple sclerosis. The Neurologist 13 (2), 57–72.

Roosendaal, S. D., Schoonheim, M. M., Hulst, H. E., Sanz-Arigita, E. J., Smith, S. M., Geurts, J. J. G., Barkhof, F., Jun 2010. Resting state networks change in clinically isolated syndrome. Brain 133 (Pt 6), 1612–1621.

Rousseeuw, P. J., Driessen, K. V., 1998. A fast algorithm for the minimum covariance determinant estimator. Technometrics 41, 212–223.

Rovira, A., Swanton, J., Tintore, M., Huerga, E., Barkhof, F., Filippi, M., Frederiksen, J. L., Langkilde, A., Miszkiel, K., Polman, C., Rovaris, M., Sastre-Garriga, J., Miller, D., Montalban, X., May 2009. A single, early magnetic resonance imaging study in the diagnosis of multiple sclerosis. Archives of Neurology 66 (5), 587–592.

Sailer, M., Fischl, B., Salat, D., Tempelmann, C., Schönfeld, M. A., Busa, E., Bodammer, N., Heinze, H.-J., Dale, A., Aug 2003. Focal thinning of the cerebral cortex in multiple sclerosis. Brain 126 (Pt 8), 1734–1744.

Salvador, R., Suckling, J., Coleman, M. R., Pickard, J. D., Menon, D., Bullmore, E., Sep 2005. Neurophysiological architecture of functional magnetic resonance images of human brain. Cereb Cortex 15 (9), 1332–1342.

Shirer, W. R., Ryali, S., Rykhlevskaia, E., Menon, V., Greicius, M. D., May 2011. Decoding subject-driven cognitive states with whole-brain connectivity patterns. Cereb Cortex(in press).

Song, S.-K., Sun, S.-W., Ju, W.-K., Lin, S.-J., Cross, A. H., Neufeld, A. H., Nov 2003. Diffusion tensor imaging detects and differentiates axon and myelin degeneration in mouse optic nerve after retinal ischemia. Neuroimage 20 (3), 1714–1722.

Stark, D., Margulies, D., Shehzad, Z., Reiss, P., Kelly, A., Uddin, L., Gee, D., Roy, A., Banich, M., Castellanos, F., Milham, M., 2008. Regional variation in interhemispheric coordination of intrinsic hemodynamic fluctuations. Journal of Neuroscience 28, 13754—-13764.

Swanton, J. K., Rovira, A., Tintore, M., Altmann, D. R., Barkhof, F., Filippi, M., Huerga, E., Miszkiel, K. A., Plant, G. T., Polman, C., Rovaris, M., Thompson, A. J., Montalban, X., Miller, D. H., August 2007. Mri criteria for multiple sclerosis in patients presenting with clinically isolated syndromes: a multicentre retrospective study. Lancet Neurology 6 (8), 677–686.

Trapp, B. D., Peterson, J., Ransohoff, R. M., Rudick, R., Mork, S., Bo, L., Jan. 1998. Axonal transection in the lesions of multiple sclerosis. N Engl J Med 338 (5), 278–285.

Tzourio-Mazoyer, N., Landeau, B., Papathanassiou, D., Crivello, F., Etard, O., Delcroix, N., Mazoyer, B., Joliot, M., 2002. Automated anatomical labeling of activations in SPM using a macroscopic anatomical parcellation of the MNI MRI single-subject brain. NeuroImage 15, 273–289.

Valsasina, P., Rocca, M. A., Absinta, M., Sormani, M. P., Mancini, L., De Stefano, N., Rovira, A., Gass, A., Enzinger, C., Barkhof, F., Wegner, C., Matthews, P. M., Filippi, M., Apr 2011. A multicentre study of motor functional connectivity changes in patients with multiple sclerosis. Eur J Neurosci 33 (7), 1256–1263.

Vercellino, M., Masera, S., Lorenzatti, M., Condello, C., Merola, A., Mattioda, A., Tribolo, A., Capello, E., Mancardi, G. L., Mutani, R., Giordana, M. T., Cavalla, P., May 2009. Demyelination, inflammation, and neurodegeneration in multiple sclerosis deep gray matter. J Neuropathol Exp Neurol 68 (5), 489–502.

Weil, R. S., Rees, G., Dec 2010. Decoding the neural correlates of consciousness. Curr Opin Neurol 23 (6), 649–655.

Weygandt, M., Hackmack, K., Pfüller, C., Bellmann–Strobl, J., Paul, F., Zipp, F., Haynes, J., Jun. 2011. Mri pattern recognition in multiple sclerosis normal-appearing brain areas. PLoS ONE 6 (6), e21138–e21138.

Wylezinska, M., Cifelli, A., Jezzard, P., Palace, J., Alecci, M., Matthews, P. M., 2003. Thalamic neurodegeneration in relapsing-remitting multiple sclerosis. Neurology 60 (12), 1949–1954.

Yaldizli, O., Glassl, S., Sturm, D., Papadopoulou, A., Gass, A., Tettenborn, B., Putzki, N., Dec 2011. Fatigue and progression of corpus callosum atrophy in multiple sclerosis. J Neurol 258 (12), 2199–2205.

Yan, H., Zuo, X.-N., Wang, D., Wang, J., Zhu, C., Milham, M. P., Zhang, D., Zang, Y., Oct 2009. Hemispheric asymmetry in cognitive division of anterior cingulate cortex: a resting-state functional connectivity study. Neuroimage 47 (4), 1579–1589.

Zhu, B., Moore, G. R., Zwimpfer, T. J., Kastrukoff, L. F., Dyer, J. K., Steeves, J. D., Paty, D. W., Cynader, M. S., Apr 1999. Axonal cytoskeleton changes in experimental optic neuritis. Brain Res 824 (2), 204–217.

Supplementary Material for Richiardi et al.'s manuscript

1. Data processing and modelling

This section gives more details about the pattern recognition methodology used in the paper, and points to available open-source code to reproduce the method.

1.1. Data preprocessing

Figure 1 provides an overview of the main processing and modelling steps constituting our method. All steps up to the regional averaging step are performed using a combination of tools from the SPM package[1] and custom code. All necessary custom code up to the dependency computation step are open source and available as part of the author's *connectivity decoding toolkit*, available at `http://miplab.epfl.ch/richiardi/software.php`.

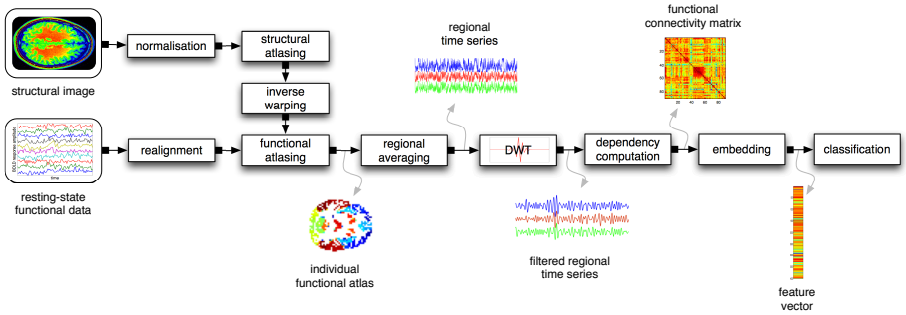

Supplementary Figure 1: Main data processing and modelling step for our method.

1.2. Embedding connectivity graphs for classification

In our approach, the last step before classification is to represent the graph in a vector space, so that statistical machine learning techniques can be used. The reason for using an embedding approach to graph classification is that atlased brain connectivity graphs are part of a restricted class of graphs, because the vertices correspond directly to the atlas' regions (Richiardi et al., 2010, 2011). Thus, there is no need to solve the *vertex correspondence problem* between graphs, which is where most of the complexity resides in *graph matching* algorithms. We thus resort to a *graph embedding* approach called direct embedding (Richiardi et al., 2010, 2011), whereby the upper-triangular part of the adjacency matrix of each graph is represented in a vector space, and each connection of the functional connectivity graph corresponds to a dimension of the vector space.

[1] available at `http://www.fil.ion.ucl.ac.uk/spm/`

1.3. Classification technique

The feature vector representation of each subject's connectivity graph can be used in a classification setting to discriminate control and patients. The function that predicts patient or control status from data is called a classifier. The parameters of the function can be learned from data by using a large number of well-known statistical machine learning methods, including (among others) support vector machines (Mourao-Miranda et al., 2005). The classification problem can be seen as a high-dimensional learning task, because there are many more features (dimensions) in the vector space than training samples. To reduce the problem of overfitting in such situations, we use a multiple-classifier system. The principle is to train a set of *base classifiers*, each performing above chance but not necessarily very accurate, and to obtain a final discriminant function by combining (*ensembling*) the outcomes of the base classifiers; e.g., using a voting mechanism. This scheme is often combined with bootstrap aggregation or "bagging", where each base classifier is trained on a resampled version of the original training set (Breiman, 1996). Here, we use functional tree (FT) classifiers (Gama, 2004) as base classifier. They are similar to a classical decision tree, but allow decision leaves to be replaced by a multivariate regression function. Furthermore, the regression function itself is boosted by using the LogitBoost algorithm (Friedman et al., 2000), an approach that focuses learning on the most difficult samples and greatly improves accuracy. The use of 21 FT classifiers and their combination via bagging enables a satisfactory tradeoff between good accuracy and generalisation capability.

1.4. Computation of discriminative weights

For our particular classifier (ensemble of FTs), each base classifier recursively partitions the feature space by selecting the most discriminative feature to split the data into controls and patients at each level of the tree. Thus, the fact that a feature is selected in a the decision tree is an indication of merit relative to other non-selected features. Furthermore, since a regression is formed in each base classifier, the regression weight coefficient attached to the feature is proportional to its importance for the discrimination task. By summing regression weights for each feature between the 21 base classifiers of each fold, we can obtain a measure of the *discriminative weight* of the selected connections. We combine per-fold estimates of the discriminative weights of features by using a weighted sum across folds, where the weight is proportional to the accuracy in each fold. Thus, the weight assigned to features by a classifier that did not result in correct prediction will not count towards the total discriminative weight.

Finally, we use a non-parametric permutation testing approach to decide which features should be considered as having a significant discriminative weight (Nichols and Holmes, 2002; Mourao-Miranda et al., 2005). To this end, we generate 20 random permutations of the class labels (control or patient), and run cross-validation experiments. We use a threshold at significance level 5% corrected for multiple comparisons. This results in a set C of discriminative connections.

2. Details of patients and controls in the study sample

Supplementary Table 1 contains details of the demographics of the study sample. A summary of this table is provided in Table 1.

	ID	gender	age (y)	EDSS	ll (cm^3)	dd (y)	na	type	treatment	classified?
patients ($N = 22$)	1	F	43	1.5	0.55	1.0	1	On	Copaxone	yes
	2	M	42	2.5	4.53	8.4	7	SePyCeBs,Se, Se,Se,Se,SePy, SePyBs	none	yes
	3	M	29	1.5	5.98	5.7	6	SePy,On,Bs,Se,Vi,On	Rebif 3x44	no
	4	M	43	1.5	0.52	9.6	3	Vi,Se,SePy	Rebif 3x44	yes
	5	F	34	2.5	2.80	8.6	12	Se,Se,Se,SePy,Bs,My,?,?,?,Se,?,Bs,SePy,Bs,My	Rebif 3x44	yes
	6	F	28	1.5	2.56	3.4	5	Bs,Em,SePy,My,My	Betaferon	no
	7	F	34	2	6.11	9.0	4	Se,Se,SeMy,?	none	yes
	8	F	36	2	4.71	0.7	1	SeBs	Betaferon	yes
	9	F	32	1.5	1.93	3.8	1	My	none	yes
	10	M	40	1.5	1.50	7.1	2	MyOn,My	Rebif 3x44	yes
	11	F	27	1.5	2.20	6.8	3	Vi,ViSe,On	none	yes
	12	F	37	2	0.24	0.5	2	My,EmOn	none	yes
	13	M	38	2	0.39	0.7	1	OnMy	none	no
	14	F	21	2.5	0.00	1.2	2	Em,SeBs	none	yes
	15	F	51	2.5	5.88	8.9	6	Vi,Se,Bs,Se,Se,SeBs	Rebif 3x44	yes
	16	F	55	2.5	6.08	1.4	3	On,Bs,My	Betaferon	yes
	17	F	33	1.5	2.96	1.7	2	My,Py	none	yes
	18	F	28	1.5	14.29	5.8	5	Se,CeBs,Se,Py,SePy	Betaferon	yes
	19	M	42	2	2.30	8.9	2	Bs,SeBs	none	yes
	20	M	39	2.5	2.77	8.6	7	SePy,SePy,Bs,Se,SeCe,SeCeBs	Copaxone	yes
	21	M	32	1.5	0.10	1.1	2	My,My	none	yes
	22	F	44	2.5	0.51	1.3	1	OnSe	none	no
controls ($N = 14$)	1	M	32	-	-	-	-	-	-	yes
	2	M	42							yes
	3	M	45							yes
	4	M	42							yes
	5	F	44							yes
	6	F	43							yes
	7	F	42							yes
	8	M	35							yes
	9	F	32							no
	10	F	46							yes
	11	F	33							yes
	12	F	29							yes
	13	F	31							yes
	14	F	41							no

Supplementary Table 1: Overview of the patients and controls with their demographics and clinical measures. *dd* stands for disease duration. *na* stands for number of attacks. *type* stands for the type of each attack. The attack types are coded as follows: *Se*=Sensitive, *Py*=pyramidal, *Bs*=brainstem, *Ce*=Cerebellar, *My*=myelitis, *On*=Optic neuritis, *Vi*=visual, *Em*=Eye movements (cranial nerve neuritis or internuclear ophtalmoplegia), *?*=not known

3. Atlas regions and nodes of the default-mode network

Supplementary Table 2 contains details of the atlas regions of interest, and Supplementary Table 3 contains the definition of the default-mode network (Buckner et al., 2008).

Lobe	Region	Short name
Frontal	Precentral	PreCen
	Frontal Sup	FrSup
	Frontal Sup Orb	FrSupOrb
	Frontal Mid	FrMid
	Frontal Mid Orb	FrMidOrb
	Frontal Inf Oper	FrInfOp
	Frontal Inf Tri	FrInfTr
	Frontal Inf Orb	FrInfOrb
	Rolandic Operculum	RolOp
	Supp Motor Area	SupMotor
	Olfactory	Olfac
	Frontal Sup Medial	FrSupMed
	Frontal Mid Orb Medial	FrMidOrbMed
	Rectus	Rec
Limbic + Insula	Insula	Ins
	Cingulum Ant	Acc
	Cingulum Mid	Mcc
	Cingulum Post	Pcc
	Hippocampus	Hipp
	Parahippocampal	ParaHipp
	Amygdala	Amyg
Occipital	Calcarine	Cal
	Cuneus	Cun
	Lingual	Lin
	Occipital Sup	OccSup
	Occipital Mid	OccMid
	Occipital Inf	OccInf
	Fusiform	Fus
Parietal	Postcentral	PostCen
	Parietal Sup	ParSup
	Parietal Inf	ParInf
	Supramarginal	SupMarg
	Angular	Ang
	Precuneus	Prec
	Paracentral Lobule	ParCenLob
Subcortical (DGM)	Caudate	Caud
	Putamen	Put
	Pallidum	Pal
	Thalamus	Thal
Temporal	Heschl	Hes
	Temporal Sup	TempSup
	Temporal Pole Sup	TempPole
	Temporal Mid	TempMid
	Temporal Pole Mid	TempPolMid
	Temporal Inf	TempInf

Supplementary Table 2: 90 regions subset of the AAL atlas (Tzourio-Mazoyer et al., 2002) and their grouping in lobes. All regions are bilateral. *DGM*: deep grey matter.

DMN node	AAL regions (all bilateral)
Ventral and medial prefrontal cortex	Superior frontal orbital, middle frontal orbital, medial frontal, gyrus rectus, anterior cingulate
Posterior cingulate and retrosplenial cortex	Posterior cingulate, precuneus
Inferior parietal lobule	Parietal inferior, angular gyrus
Lateral temporal cortex (BA 21)	Middle temporal gyrus, middle temporal pole
Hippocampal formation	Hippocampus and parahippocampal gyrus

Supplementary Table 3: Regions included as nodes of the default-mode network (DMN) (Buckner et al., 2008) in terms of the AAL atlas, similar to the correspondence established by Fransson and Marrelec (2008).

4. Full list of connections in the discriminative graph

Supplementary Table 4 shows the list of connections that make up the discriminative graph as well as their discriminative weight. It also shows the weights that go into computing the two summary indices of connectivity alterations of Section 1.5.

Supplementary Figure 2 shows a visualisation of the relative discriminative weights of the 50 highest-weighted connections of the discriminative graph.

Connection	Discriminative weight	RCI weight	ICI weight
CaudL - TempPolMidR	2.04	0.018	
AmygR - TempPoleR	1.93		0.137
FrInfOrbL - TempPolMidR	1.85	0.017	
RolOpR - FusL	1.76	0.016	
PccL - PrecL	1.71	0.016	
ParSupR - PurR	1.64	0.015	
SupMotorL - RecR	1.62	0.015	
FrSupOrbL - TempPolMidR	1.60	0.014	
SupMotorL - PalL	1.50	0.014	
FrMidL - HesL	1.48	0.013	
FrSupMedL - PrecL	1.48	0.013	
SupMotorL - RecL	1.35	0.013	
ThalL - TempPoleR	1.34		0.132
FrSupMedL - TempPolMidR	1.29	0.012	
RolOpR - CalL	1.25	0.012	
AmygR - HesR	1.25		0.121
HippR - TempPoleR	1.23		0.067
AmygR - TempPolMidL	1.19		0.067
PreCenL - PostCenL	1.16	0.011	
ParSupR - SupMargL	1.16	0.011	
ParSupR - PalL	1.15	0.011	
FrSupOrbR - TempPolMidR	1.11	0.011	
HesL - TempPoleR	1.11	0.011	
ParCenLobL - PalL	1.04	0.010	
FrMidOrbR - RecR	1.04	0.010	
PreCenL - HesL	1.02	0.010	
AccL - CaudL	1.02	0.009	
FrMidOrbR - PalR	1.02	0.009	
OccSupR - PalL	1.00	0.009	
FrMidOrbMedL - PalL	1.00	0.009	
HippR - PutL	0.99	0.009	
FrSupOrbL - AccR	0.98	0.009	
PreCenL - PostCenR	0.96	0.009	
PreCenR - TempPolMidR	0.94	0.009	
FrMidOrbR - PurR	0.94	0.009	
FrMidOrbL - PalR	0.94	0.008	
RecL - TempInfL	0.93	0.008	
ParaHippR - AmygR	0.92		0.064
SupMotorR - RecL	0.91	0.008	

Connection	Discriminative weight	RCI weight	ICI weight
ParSupL - ParCenLobL	0.91	0.008	
ParSupR - PutL	0.90	0.008	
ParaHippR - TempInfR	0.88	0.008	
FrSupMedL - TempPoleL	0.88		0.062
RecR - TempPoleR	0.88	0.008	
FrInfOrbL - HippR	0.86	0.008	
FrSupL - HesR	0.86	0.008	
ParaHippL - ThalR	0.85		0.061
FrMidL - RecR	0.84	0.008	
InsL - CunL	0.84	0.008	
ParaHippR - FusR	0.84	0.008	
AmygR - TempInfL	0.83	0.008	
PostCenL - ParInfL	0.83	0.008	
OccInfL - TempInfL	0.83	0.008	
AmygR - TempPolMidR	0.83	0.007	
FrInfTrL - TempMidL	0.82	0.007	
HesL - TempPoleL	0.82	0.007	
OccInfR - PalL	0.82	0.007	
ParCenLobR - PalL	0.82	0.007	
ParaHippR - ThalL	0.81	0.007	
FrInfTrL - PrecL	0.81	0.007	
PalL - TempInfR	0.79	0.007	
HippL - PalL	0.79	0.007	
HippR - OccInfR	0.78	0.007	
FrInfTrL - ParSupR	0.77	0.007	
RolOpR - LinL	0.74	0.007	
OccInfR - PurR	0.74	0.007	
RolOpR - ParSupR	0.74	0.007	
FrSupMedR - ParCenLobR	0.73	0.007	
AccL - TempPolMidR	0.73	0.007	
AccR - TempPolMidR	0.72	0.007	
FrInfOpL - ParaHippL	0.72	0.007	
FrMidL - TempPolMidR	0.67	0.007	
AccL - ParaHippL	0.67		0.059
AngL - PrecL	0.64	0.007	
SupMotorL - ParaHippL	0.64	0.006	
RecR - HippR	0.64	0.006	
RolOpR - CunL	0.64	0.006	
FrSupR - TempPolMidR	0.63	0.006	
RecL - TempPolMidR	0.63	0.006	
FrSupL - TempPolMidR	0.63	0.006	
ParaHippL - ThalL	0.63	0.006	
RecR - TempPolMidR	0.63	0.006	
FrSupOrbR - ThalL	0.62	0.006	
FrMidOrbL - TempPolMidR	0.62	0.006	
FrSupMedL - ParCenLobR	0.62	0.006	
ParSupR - TempSupR	0.62	0.006	
ParSupL - ParCenLobR	0.61	0.006	

Connection	Discriminative weight	RCI weight	ICI weight
OccMidL - TempPolMidR	0.61	0.006	
PostCenL - ThalL	0.61		0.058
SupMotorR - AmygL	0.61	0.006	
RecR - CaudR	0.61	0.005	
AccL - ParCenLobR	0.60	0.005	
PrecL - TempMidL	0.59	0.005	
OccMidR - HesL	0.59	0.005	
OlfacR - PalR	0.58	0.005	
AmygR - TempSupR	0.57	0.005	
ThalL - TempMidR	0.57	0.005	
PccR - PrecL	0.57	0.005	
PurR - HesR	0.57	0.005	
FrInfTrL - TempPolMidR	0.56	0.005	
TempMidR - TempInfL	0.54	0.005	
ParSupR - HesL	0.54	0.005	
FrMidOrbMedL - AngR	0.54	0.005	
FrMidOrbMedL - RecR	0.53	0.005	
FrSupL - HesL	0.53	0.005	
RolOpR - OccMidR	0.53	0.005	
FrInfTrL - TempMidR	0.53	0.005	
OccInfL - PurR	0.52	0.005	
RecR - CaudL	0.52	0.005	
FrInfTrR - TempPolMidR	0.52	0.005	
ParaHippL - CaudL	0.52	0.005	
SupMotorR - ParaHippR	0.52	0.005	
SupMotorR - ParaHippL	0.51		0.058
RecR - PutL	0.51	0.005	
FrMidOrbR - TempPolMidR	0.51	0.005	
RecR - PccR	0.50	0.005	
FrInfTrR - FrSupMedR	0.49	0.005	
FrMidOrbMedR - CaudL	0.49	0.005	
ThalL - TempSupL	0.49		0.058
AmygL - ParCenLobL	0.49	0.004	
OccSupL - TempPolMidR	0.49	0.004	
FrInfOrbL - HesL	0.48	0.004	
AngL - AngR	0.48	0.004	
RolOpR - CalR	0.48	0.004	
FrSupOrbL - PccR	0.48	0.004	
FrMidOrbMedR - AmygL	0.48	0.004	
FrSupOrbR - PccR	0.48	0.004	
CunL - AngL	0.48	0.004	
FrSupOrbL - PalR	0.48	0.004	
CunR - HesL	0.48	0.004	
PccR - SupMargR	0.48	0.004	
ParSupR - TempMidL	0.48	0.004	
OccSupR - TempPolMidR	0.48	0.004	
RecR - TempInfR	0.47	0.004	
FrMidOrbL - ParCenLobR	0.47	0.004	

Connection	Discriminative weight	RCI weight	ICI weight
RecL - ParaHippL	0.45	0.004	
PrecR - ParCenLobL	0.45	0.004	
FrMidR - ParCenLobR	0.45	0.004	
PccL - CunR	0.44	0.004	
FrInfOrbR - PalL	0.44	0.004	
FrMidOrbL - PccR	0.44	0.004	
InsL - TempPolMidL	0.44	0.004	
AccR - ParSupR	0.44	0.004	
RecL - HippL	0.44	0.004	
TempMidL - TempPolMidR	0.42	0.004	
FrMidOrbMedR - TempPolMidR	0.42	0.004	
FrMidL - ParaHippL	0.42	0.004	
FusR - PalR	0.41	0.004	
ParCenLobR - ThalR	0.40	0.004	
TempMidL - TempInfR	0.40	0.004	
LinR - PalL	0.40	0.004	
FrInfTrL - FrSupMedR	0.40	0.004	
SupMargR - ThalL	0.40	0.004	
FrInfTrR - AngL	0.40	0.004	
PostCenR - ThalL	0.39		0.057
AmygR - PostCenL	0.39	0.003	
PrecR - PalL	0.39	0.003	
CalL - TempPolMidR	0.38	0.003	
RecR - PccL	0.38	0.003	
AccL - AmygL	0.38	0.003	
PccR - ParInfR	0.38	0.003	

Supplementary Table 4: Full list of connections part of the discriminative graph, their weight, and their normalised weight in the summary indices of connectivity alterations (see Section 1.5).

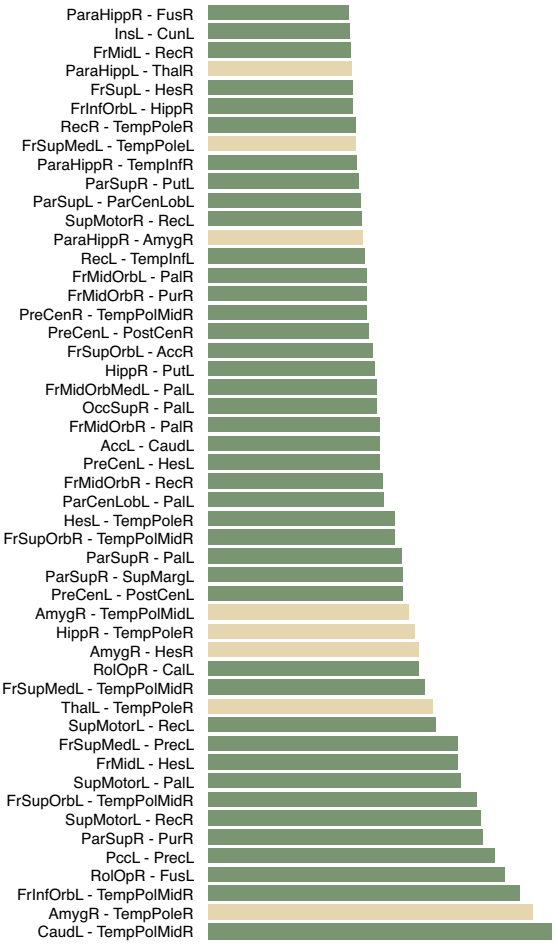

Supplementary Figure 2: Relative discriminative weight of 50 most discriminative connections amongst the 161 significant connections in the discriminative graph. Connections in olive green are on average stronger in controls than in patients, while connections in sandy yellow are stronger in patients than in controls.

5. Ipsi- and contra-lateral functional connectivity alterations

Supplementary Figure 3 shows a division of the discriminative graph into ipsi- and contra-lateral subnetworks.

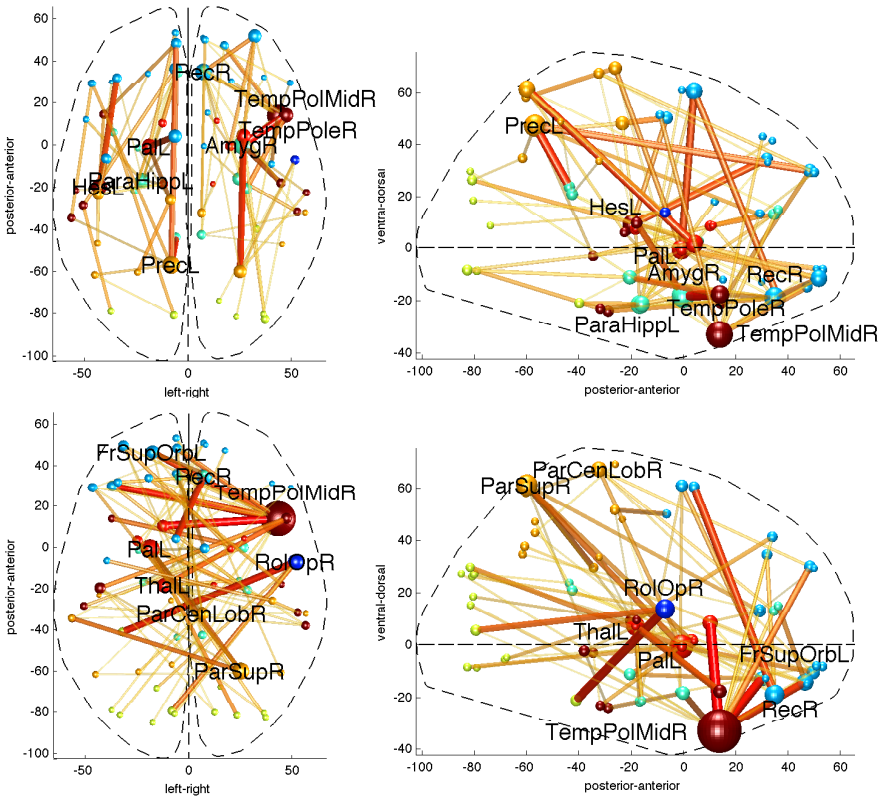

Supplementary Figure 3: Discriminative graphs for MS versus control divided into ipsilateral and contralateral components. The top row shows the subgraph containing only ipsilateral connections, while the bottom row shows the subgraph containing only contralateral connections. The size of spheres is proportional to the regional discriminative weight, and the colour indicates the lobe the regions are part of. The size and shade of connections between regions reflects their discriminative weight: stronger hues and larger sizes reflect higher discriminative weight.

6. Functional connectivity pattern of control subjects

Supplementary Figure 4 shows the average correlation values of the 100 strongest functional connections in the 0.06–0.11 Hz frequency subband, computed across the N=14 control subjects of our sample. Note that this is not a discriminative graph, as it shows the connectivity pattern of a single group. Contralateral connections to homologous regions are particularly strong in this group (as reported in Stark et al. (2008) and elsewhere).

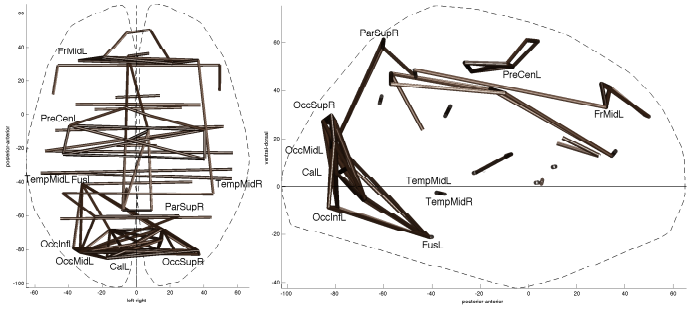

Supplementary Figure 4: Average functional connectivity in the 0.06–0.11 Hz subband for the control group, pruned to the 100 connections with the heighest weight. All connections shown are significantly different from 0 (t-test, $p<0.05$ with Bonferroni correction)

7. Performance measures for classification

Several measures of performance can be adopted, many derived from a confusion matrix (Supplementary Figure 5) which can be computed from the result of a cross-validation experiment. Confusion matrices are a common sight both in pattern recognition and in the biostatistics and epidemiology, where diagnostic tests are oven evaluated in terms of sensitivity $sens = TP/(TP + FN)$ and specificity $spec = TN/(TN + FP)$. Thus, there is a clear connection between the predictive approach and common medical practice, and understanding the results of a classification study (where sensitivity and specificity are called *class accuracies)* is intuitive to physicians.

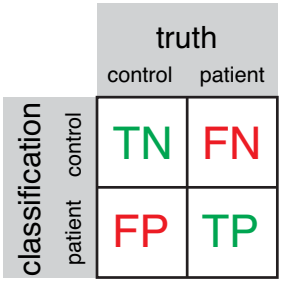

Supplementary Figure 5: Confusion matrix for assessing the outcome of a classification experiment. TN is the number of true negatives (number of controls correctly predicted to be controls), TP of true positives (patients recognised as patients), FN is the number of false negatives (number of patients mistaken for controls), and FP of false positives (controls classified as patients).